Chapter 6

Searches for Radio Counterparts of Two High-energy Pulsars: Geminga and SAX J1808.8–3658

6.1 Introduction

We searched for pulsed-radio emission from Geminga at 34.5 MHz using GEETEE (see chapter 2) and from SAX J1808.8–3658 at 327 MHz using the Ooty Radio Telescope. In this section, we briefly describe radio-pulsar searches, and outline the phenomenology of these two pulsars, which are known to emit most of their radiation in X-rays or y-rays. In the later sections, we present details of our radio observations, search analysis and discuss implications of our "null" results.

6.1.1 Pulsar searches

A pulsar survey is essentially an exercise in finding signals of unknown period and dispersion measure from unknown directions in the sky. To reach the desired levels of sensitivity, usually long integrations (several minutes) per beam position are required, on the other hand, to detect fast pulsars one must have submillisecond sampling and recording of the data. Both requirements result in very long data streams taken at a beam position in the sky, repeated for all positions covering the survey area. The best technique to look for weak, periodic signals in long time sequences is Fourier analysis: the pulsed signal would show up as enhanced Fourier amplitudes at the pulse frequency (reciprocal of the pulse period) and its harmonics. One problem is that the pulse broadening due to dispersion and scattering would considerably reduce the pulsar-signal strength. While the latter cannot be helped, it is possible (and necessary) to remove the effects of dispersion to the extent possible to improve the detectability of a pulsar.

Since one does not know the DM of the pulsar to start with, the data for every field has

to be dispersed for a large number of trial DMs. One usually adopts the incoherent dedispersion technique for this procedure, as it is less demanding on computing power. As explained above, at each position the observing band is split into a number of frequency channels and the signal over each channel is detected, integrated for a pre-set "sampling" time (usually ~ 0.1 ms); then sampled and recorded. The recording is continued for the desired integration time at the beam position. This is repeated at all beam positions.

6.1.2 Geminga Pulsar

Geminga, was detected as a gamma-ray source by SAS-2, a gamma-ray mission by NASA, in 1973. The object became an enigma since there was no radio emission seen from this object, as opposed to the well-known gamma-ray emitter pulsars, *viz.* the Crab and Vela. The little interstellar absorption seen in its soft X-ray spectrum ($\leq 1keV$) suggested a small distance, ~ 100 pc (Bignami, Caraveo, & Lamb, 1983). Optical searches from Palomar yielded no counterpart, which, in an unabsorbed region of the Galaxy, indicated $L_X/L_{opt} \gg 1$, an underluminous object. Drawing from the analogies with the Vela pulsar, it was suspected to be a neutron star.

The real breakthrough came with the observations by ROSAT[1], in 1991. Due to low background and more source-counts in the soft X-rays, it was ideal to study Geminga at those energies. A clear periodicity of ~ 237 ms was evident in the data, typical of a middle-age pulsar. The observed pulsed fraction was 25% in the soft band (≤ 0.2 keV) and reduced further in the hard X-ray band.

It was now possible to look at y-ray data from EGRET[2] to study pulsation. EGRET not only confirmed the periodicity, but also provided the first estimate of $\dot{P}$ by virtue of its long-term observations. The theoretical estimates for the neutron-star parameters were then possible: magnetic field $B_s \sim 1.5 \times 10^{12}$ G, spin-down age $\tau \sim 3.4 \times 10^5$ yr, energy loss $\dot{E} \sim 3.2 \times 10^{34}$ erg/s, etc.

Deep optical searches yielded the optical counterpart (1992), and the comparison of the image with the earlier observations, made in 1984, led to a preliminary value for its proper motion, ($\sim 0.17''$/yr), surprisingly close to the earlier expectations. Hubble Space Telescope observations, in 1995, allowed a parallax measurement of this source, which led to the distance estimation of 157^{+59}_{-34}pc (Caraveo et *al.*, 1996)

When the paralactic and proper motion of the optical counterpart were taken into account,

[1]The Roentgen Satellite, ROSAT, was a telescope for observations in the soft X-ray band.

[2]Energetic Gamma-ray Experiment Telescope on board Compton Gamma-Ray Observatory (CGRO), working in the energy range of 20-30,000 MeV.

the EGRET data resulted in a noticeably improved model for the arrival time of pulses from the pulsar. Thus, the y-ray pulses could be attributed to the same object!

Geminga's nature as a relatively young, isolated neutron star (INS) is well established. This gamma-ray pulsar is the third strongest gamma-ray source in the sky, and shows very stable pulsed emission. It is the only pulsar in the catalog of pulsars by Taylor, Manchester, & Lyne (1995) which does not have confirmed radio pulsations.

Geminga emits copious energy in y-rays ($\geq 10^{34}$ erg/s), and the best data on Geminga is obtained from observations in this energy band. The EGRET spectrum in the energy interval between 30 MeV and 2 GeV is well-fitted by a power law with photon spectral index -1.5 ± 0.08, and a definite roll-off between 2-4 GeV is reported. The light curves for different energy intervals are shown in figure 6.1.

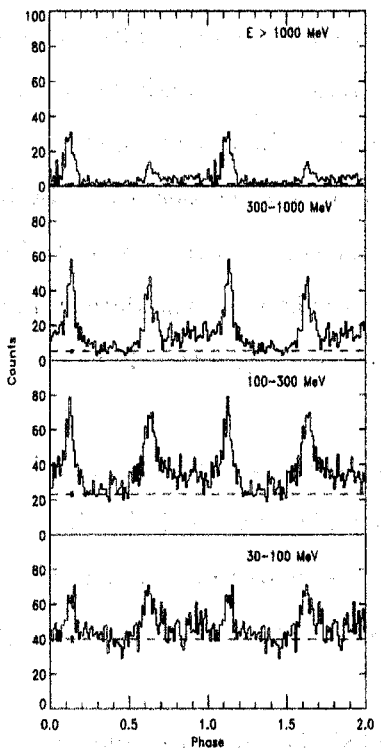

Figure 6.1: Light curves of Geminga using EGRET. The pulse is very wide, and there is an interpulse roughly 180° away from the main pulse. There are significant spectral differences present among the pulse components. It is also evident, that the analysis of the Geminga light curve leaves no room for any unpulsed y-ray emission (from Mayer-Hasselwander et *al.*, 1994).

Results of EGRET timing analysis for Geminga are:

$$\mathrm{P} = 237.09778498637 \text{ msec} \tag{6.1}$$

$$\dot{P} = 1.097358 \times 10^{-14} s/s \tag{6.2}$$

$$\alpha = 6^h 33^m 54^s.1 \quad (6.3)$$

$$\delta = 17°46'12".1 \quad (6.4)$$

at an epoch of TO=2448750.5 JD.

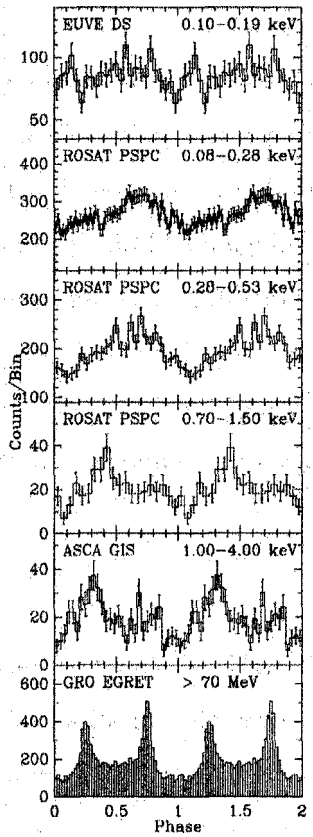

Figure 6.2: Pulse profiles of all the available soft X-ray data on Geminga, folded over a duration twice the known pulse period, from Halpern & Wang, 1997. The EGRET light curve in the gamma-rays is shown for comparison (From Mattox, Halpern, & Caraveo, 1996).

The light curves observed in X-rays with the Extreme Ultra-violet Explorer (EUVE), ROSAT, and ASCA[3] are shown in figure 6.2, along with the EGRET curve for comparison. The shape of the light curve shows a noticeable change with energy. The structure in the light curve observed by EUVE and ROSAT ($\leq 0.7\,\mathrm{keV}$) is not statistically very significant and the pulsed fraction increases toward higher energies. The ROSAT light curve in the band 0.7–1.5 keV matches well with the ASCA curve, which in turn appears close to the EGRET light curve. It was noted that there is a qualitative change in the light curve at energy $\sim 1\,\mathrm{keV}$.

The soft X-rays originate from a hot surface, which is a significant fraction of the neutron star's surface. ASCA data reveals a highly pulsed profile with a secondary peak, and the spectrum

[3] Advanced Satellite for Cosmology and Astrophysics (ASCA), telescope working in the hard X-ray band.

reveals a non-thermal component. The change in the light curve around 1 keV is probably related to such a component. Details of such a non-thermal process have been related to the lack of radio emission from Geminga (Halpern & Ruderman, 1993).

The Geminga Fraternity?

Although we have no confirmed radio emission from Geminga (except the recent claims, which we discuss soon), it belongs to a well-known fraternity of INSs in our galaxy that emit in the high energy window. Several such INSs are known by now, but they still form a minority compared to the radio-pulsar population. But, Geminga could be a prototype of a population of INSs which are radio-silent, bright in y-rays, conspicuous in X-rays, and weak in optical band (Caraveo, Bignami, & Trümper, 1996). A few detections of such pulsating sources in the EGRET data and other recently discovered neutron stars [RX J1856.5-3754 (Walter, Wolk, & Neuhauser, 1996), the point source at the center of Cas-A discovered by Chandra[4], are typical examples] support this point of view.

Why Not a Radio Pulsar?

Out of seven pulsars detected by EGRET, all but Geminga were previously known to be radio pulsars. So it is natural to ponder over the question: Why is Geminga not a radio emitter? Two general possibilities have been considered: (a) An unfavorable beaming of the radiation, or (b) A genuine lack of radio emission in this system due to magnetospheric conditions. A detection of radio emission, or stringent upper limits on such a radiation, could help to understand the pulsar geometry and/or its non-thermal emission. Over the years, various searches for pulsed radio emission from Geminga have been carried out (Mandolesi *et* al., 1978, Mayer-Hasselwander *et* al., 1979, Seiradakis, 1981, Manchester & Taylor, 1981), with null results.

Recently, three Russian groups simultaneously announced detection of radio pulsations from Geminga at frequency close to 102 MHz (see table 6.3). Following their announcement, several new searches for radio emission, pulsed or otherwise, followed. No other confirmation (see table 6.1, table 6.2), except for another tentative detection at 102 MHz (Vats *et* al., 1999), is reported to date.

Deep searches at frequencies higher than 100 MHz constrain the power-law spectral index of radio emission above 100 MHz to be $-7.6 \leq a \leq -3.6$. Another search at 35 MHz and 327 MHz

[4] Chandra, an X-ray imaging instrument, combines an efficient sub-arcsecond resolution with a suite of advanced imaging and spectroscopic instruments.

produced a null result (Ramachandran, Deshpande, & Indrani, 1998), and these upper limits put severe constraints on the pulsed radio emission from this pulsar.

Radio Frequency MHz	Upper Limit mJy	reference
74	56 (2σ)	Kassim & Lazio, 1999.
326	5 (2σ)	Kassim & Lazio, 1999.

Table 6.1: Search for continuum radio emission from Geminga after the claims by Russian astronomers of a radio pulsar detection.

Geminga Search: Our motivation

We tabulate here all the successes and failures in radio detections reported in literature.

It is clear from the tabulated results, that (1) Geminga radio emission was reported to be detectable only close to 100 MHz., (2) The spectrum, both below and above 100 MHz would have to be extremely steep (if one assumes that the 100 MHz detections were valid), $\mid a \mid \geq -2.0$), **(3)** Even from the various claims of detections, the radio flux appears to be highly variable, and may vary between 5-500 mJy at 100 MHz.

Already sensitive upper limits are available at 34.5 MHz. We searched for possible pulsations again at 34.5 MHz when the pulsar was apparently a strong source of pulsations at 102 MHz. Such simultaneous observations at 102 MHz and other frequencies could help in improving detectability that may be otherwise suffering from any time variability of Geminga flux due to internal and due to interstellar scintillation effects. One may expect, in general, a correlation between an enhanced emission at 102 MHz, and that observable at 35 MHz. With this view, we proposed simultaneous observations at 35 MHz and 102 MHz. The observations at 102 MHz were made at Puschino using the BSA array (Izvekova et *al.*, 1979), whereas observations at 35 MHz were carried out using GEETEE. Since both, the GEETEE and BSA arrays are transit instruments, the actual observation time differed by ~ 2.5 hours, providing at best near-simultaneous pairs of observations.

Radio Frequency MHz	Upper Limit for flux density mJy	reference
35	100	Ramachandran, Deshpande & Indrani, 1998.
327	0.3	Ramachandran, Deshpande & Indrani, 1998.
317	3	McLaughlin, M. A. et *al.*, 1999.
318	0.1	Burderi, Fauci & Boriakoff, 1999.
430	0.07	Burderi, Fauci & Boriakoff, 1999.
1400	0.07	Burderi, Fauci & Boriakoff, 1999.

Table 6.2: Searches for the pulsed radio emission from Geminga.

6.1.3 SAX J1808.8–3658, an X-ray binary millisecond pulsar

The transient X-ray burst source SAX 51808.8–3658 was discovered (in't Zand, et al., 1998) in September, 1996, using satellite BeppoSAX, when two X-ray bursts were recorded. RXTE detected a positionally coincident object, XTE 51808–369 during 1998, and coherent pulsations at $\sim$ 401 Hz were detected during this X-ray burst (Chakrabarty & Morgan, 1998, and Wijnands & van der Klis, 1998). These observations further allowed the measurements of an orbital period of about 2 hr and other parameters. This detection of a binary milli second X-ray pulsar appears to dramatically confirm the link between the low mass x-ray binaries (LMXBs) and the radio millisecond pulsars (MSPs) proposed more than a decade ago.

The source was classified as a low Mass X-ray Binary (LMXB) system, containing a low-magnetic field neutron star accreting matter from a companion star of less than one solar mass, with a probable distance of 4 kpc. The issues dealing with the X-ray binary systems and millisecond pulsar formation were reviewed by Bhattacharya & van den Heuvel, 1991.

SAX 51808.8–3658 is categorized as a soft X-Ray transients source (SXRT), a subclass of

Flux density mJy	reference
100	Kuz'min & Losovskii, 1997.
8^{+3}_{-2}	Shitov & Pugachev, 1998.
60 ± 95 (5-500)	Malofeev & Malov, 1997.
1000	Vats et al., 1999.

Table 6.3: All the claimed detections of Geminga at $\sim$ 102 MHz.

LMXBs. The X-ray outbursts of SXRTs are often accompanied by an burst in optical emission from the system (novæ). Increases up to $\sim$ 6 rnagnitudes *w.r.t.* their quiescent state have been measured, which have greatly assisted the identification of optical counterparts. Studies of optical novæ and their behavior in quiescence have shown that SXRTs contain late type stars (6- or 7K-type stars) and in some cases allowed a determination of the orbital period. These are known in seven systems and are in the range from 4 to 19 hours, similar to LMXBs. The mass function was measured only in the case of Cen X-4 so far (found to be $\sim 0.2 M\odot$).

Unpulsed radio emission has been observed during the outbursts of sources A1742-289, Aql X-1, and Cen X-4, but searches for a pulsed emission resulted in no detection. SXRTs are located in the galactic plane and their presence in globular clusters is of particular interest due to their possible evolutionary link with recycled MSPs, which have a tendency of being found in globular clusters at higher frequency.

An excellent review of SXRTs is available in Campana et al., 1998a.

SAX 1808.8-3658: our motivation

After the discovery of the transient X-ray source SAX J1808.8–3658, the source was observed using the Proportional Counter Array (PCA) on board RXTE on 11 April 1998. Chakrabarty & Morgan (1998) and Wijnands & van der Klis (1998) have reported persistent, coherent pulsations present

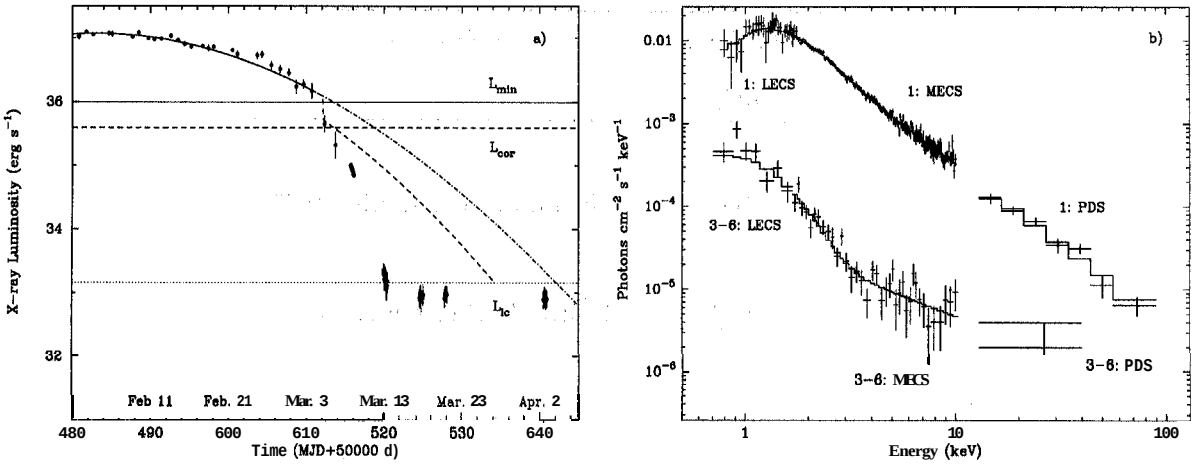

Figure 6.3: On the **left:** Light curve of the 1997 February/March outburst of Aql X-1, the scale on the Y-axis is the X-ray luminosity (in erg/s) plotted on a logarithmic scale. The data were collected with the RXTE (210 keV) and the BeppoSAX (1.510 keV), respectively. The dot-dashed line and dashed line are model fits. The horizontal solid line represents the X-ray luminosity corresponding to the closure of the centrifugal barrier L_min (for a magnetic field of 10^8 G and a spin period of 1.8 ms), and the horizontal dashed line represents the luminosity gap due to the action of the centrifugal barrier, L_{cor}. The horizontal dotted line marks the minimum. On the **right:** BeppoSAX unfolded spectra of Aql X-1 during the early stages of the fast decline and during the quiescent phase. The best-fit spectral model (blackbody plus power law) is superimposed on the data (both figures from Campana et *al.*, 1998).

in the data of frequency $\sim$ 401 Hz. The source reached a peak luminosity of 5×10^{36} erg/s and then faded below 10^{35} erg/s after a couple of days. Figure 6.4 displays the folded pulse profile of the milli-second pulsar, using RXTE data in the energy band of 2-30 keV and a period of 2.49 ms. The pulse-profile form is sinusoidal to a high degree, and the Fourier spectrum of the time series does not display any detectable higher harmonics.

The peak observed flux suggests a low magnetic field ($< 10^8$ G). The binary parameters of the system can be computed by using the timing information in the X-ray observations. Table 6.4 displays the information in a concise form. The error in the value of P constrain the positional uncertainty of the source. The pulsar mass function, which relates the pulsar mass m_1, companion mass m_2, and the binary inclination angle i (the angle between the line-of-sight and the orbital angular momentum vector), may be computed from the Keplerian parameters $a_1 sin\, i$ and P_{orb}, where a_1 & P_{orb} are the semimajor axis and orbital period of the binary;

$$\mathrm{f1} \equiv \frac{(m_2 sin\, i)^3}{(m_1 + m_2)^2} = \frac{4\pi^2 (a_1 \sin i)^3}{G {P_{orb}}^2} \tag{6.5}$$

from which the mass function obtained was $f_1 = 3.7789(2)$ x $10^{-5} M\odot$. For reasonable values of the neutron star and a random distribution of i, Chakrabarty & Morgan (1998) find the mass of

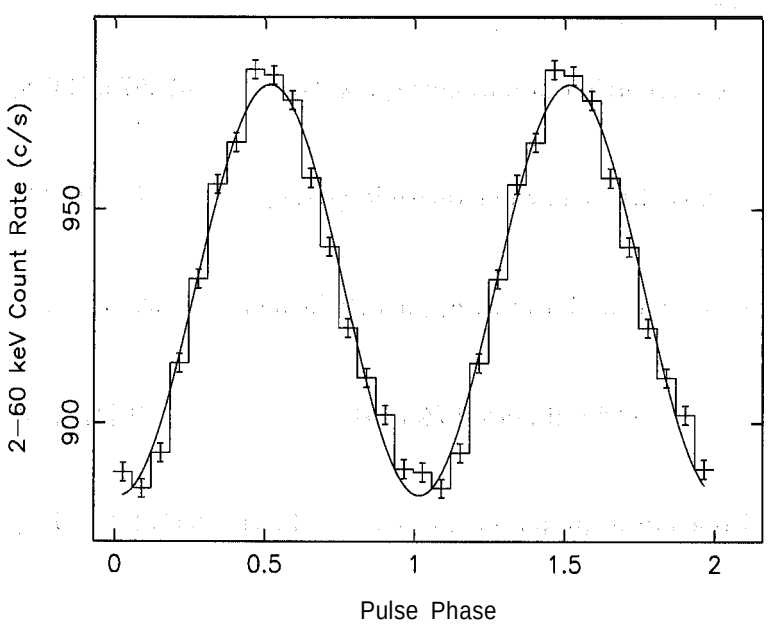

Figure 6.4: SAX J1808.8–3658: The 2–60 keV light curve folded at the 2.49 ms period, where two cycles are plotted for clarity. The solid line is the best-fitting sinusoidal. Fitting the folded light-curve with a harmonic series, the first two higher harmonics (at 800 and 1200 Hz) are $\sim 11\%$ and $\sim 4\%$ of the fundamental.

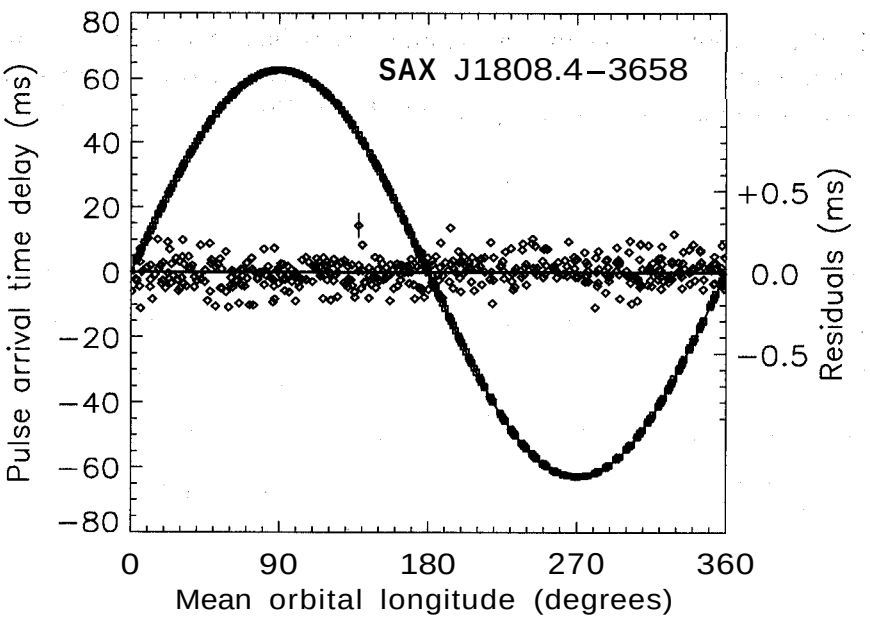

Figure 6.5: Pulse arrival time delays due to the 2-hr orbit, with respect to a constant pulse-frequency model. The mean longitude is the orbital phase age measured from the ascending node, so that the pulsar is behind the companion at 90°. Squares show the measured time delays, the solid curve is the best-fit orbital model, and the diamonds show the model residuals (on a 50x expanded scale). The residuals have an r.m.s. uncertainty of 75 μs, shown for one of the points.

Barycentric pulse frequency, ν_0 (Hz)	400.9752106(8)
Pulse frequency derivative $\lvert\dot{\nu}\rvert$(Hz/s)	$< 7 \times 10^{-13}$
Projected major axis, a_1 sini (light-ms)	62.809(1)
Orbital period, P_{orb} (s)	7249.119(1) s
Epoch of mean 90° longitude, $T_{\frac{\pi}{2}}$ (MJD)	50914.899440(1)
Eccentricity, e	$< 5 \times 10^{-4}$
Binary mass function ($M\odot$)	$3.7789(2) \times 10^{-5}$

Table 6.4: SAX J1808.8–3658 binary parameters (Chakrabarty & Morgan, 1998): Numbers in parentheses are 1a errors in the least significant digit and upper limits are quoted at 2σ level. The $\lvert\dot{\nu}\rvert$ refers to the magnitude, independent of age. Epochs refer to a barycenter dynamical time (TDB).

the binary to be $< 0.2M\odot$, and its radius $> 0.12R\odot$. This greatly constrains the nature of the binary star, which is most likely to be a low mass main-sequence star, or a white dwarf.

There is a tentative indication of a flux modulation of SAX J1808.8–3658 at its orbital period, which could be interpreted as scattering in the ablated wind. This modulation further constrains the binary inclination, and makes it highly likely that the companion mass is less than $0.1M\odot$. If there is such a scattering, broader eclipses may occur at radio wavelengths.

The observed period and magnetic fields are indeed in the range inferred for millisecond radio pulsars. Hence, once the accretion stops, it might switch on as a radio pulsar. Wijnands & van der Klis, 1998, even suggest a possible radio detection in the quiescent state of the system, if the accretion rate falls sufficiently. We considered following up this possibility. A possible radio detection from this system would be a further proof of the remarkable suggestion about the origin of the MSPs, and their progenitors. The system is probably 4 kpc away, and we estimate a DM

of $\sim 150\,pc/cm^3$ for this system from the model of galactic electron density distribution (Taylor & Cordes, 1993). A search at 327 MHz using the Ooty Radio Telescope was immediately possible. We searched this system for a possible radio pulsation using this telescope. Since pulsar activity is ruled out during X-ray outbursts from this system, we observed this source in radio when the system was believed to be its quiescent state. Our observational set-up, and other details are outlined below.

6.2 Details of the Observations

We made observations in the direction of Geminga with GEETEE at 34.5 MHz and toward SAX J1808.8–365 with the Ooty Radio Telescope (hereafter ORT) at 327 MHz. We discuss here the telescopes used and provide details of our observations.

6.2.1 Observations

We monitored Geminga at 34.5 MHz using GEETEE, where we collaborated with Dr. V. M. Malofeev, of the Puschino observatory for near-simultaneous observations of this pulsar at 111 MHz.

Geminga was monitored using GEETEE during 5–10 February, 1999, when it was observed typically twice on each day at 34.5 MHz. The duration of each observation (two on each day) was $\gtrsim 1000$ seconds on either side of the source transit time at the local meridian. On all days, pulsar B0950+08 was also observed at least once. The period and DM of this pulsar is similar to the period of Geminga and the expected value of DM for Geminga. This makes it an ideal test source to monitor system performance and the effectiveness of our search strategy.

The observations at 111 MHz were carried out at Puschino, using the Large Phased Array (BSA). Geminga was observed during 5–10 February, 1999. Pulsar B0950+08 was monitored as a test candidate for the system performance.

We searched for millisecond period pulsations in the directions of SAX 51808.8–3658 using the Ooty Radio Telescope (ORT) at 327 MHz. We also observed the millisecond pulsar B1937+21, which has a period of 1.558 ms, and a DM of $71.04\,pc/cm^3$. Being a somewhat distant and a fast pulsar with a short duty cycle, B1937+21 provides a useful test case for our observations and search algorithm.

We observed in the direction of SAX 51808.8–3658 on 12 occasions during the night of 18^{th} August, 1998, using the ORT. The X-ray transient was in its quiescent state during this period. Each one of our observations was ~ 10 minutes in duration. In table 6.5, we have noted some details of our observations. In this way, our search for pulsations in a single observation is not limited significantly by the effects of binary acceleration on the apparent pulsar periodicity. We

Observation span	**18** Aug, **1998 (12** data sets)
Integration time for each observation	$\sim$ **600** seconds
Time resolution (Hardware)	0.5/0.25 ms
Number of channels used (Bandwidth)	256 (8 MHz)
Sensitivity of the ORT (ideal 25)	15

Table **6.5:** ORT search observations of SAX **51808.8–3658** at **327** MHz. X-ray transient source was in its quiescent state.

observed SAX **51808.8–3658** over all phases of the binary for over **2** hours. Two of the **12** data sets had a time constant of **0.25** ms, whereas all others were recorded with a time constant of **0.5** ms.

6.2.2 Telescope & back-end system

Our observations of Geminga at **34.5** MHz were carried out with GEETEE, with a bandwidth of 1 MHz and our (direct voltage sampling) data-acquisition system, described in detail in chapter **2.** Here, we briefly mention the observations at **111** MHz (Russian observations of Geminga, conducted near-simultaneously with our observations at GEETEE) and Ooty Radio Telescope.

Puschino: 111 MHz observations

The Large Phased Array is a transit instrument with an operating frequency close to **102** MHz, situated at a longitude of 37°40′00" E and latitude of 54°49′00"N. The antenna array consists of **16,384** dipoles aligned in East-West direction, with total collecting area of $\approx$ **30,000** m^2. The array was upgraded recently, so that it is possible to observe sources at a frequency of **111** MHz. Observations by our collaborators were made using a multi-channel receiver, where each of the **16** channels has a frequency width of **20** kHz. The sampling time constant is **7.68** ms and the receiver time constant is **10** ms. This receiver was used by our collaborators in the near-simultaneous observations of Geminga to obtain sequences of individual pulses. The total observation time on

a point source is $3.5 sec(\delta)$ min. Pulsar B0950+08 was monitored as a test source with the same system.

Note that both the telescopes have only a limited tracking facility in hour angle. Hence, owing to the difference of longitudes between the two instruments, there was a difference of ~ 2.5 hours in the observation epochs at the GEETEE and the Puschino observatory.

Ooty Radio Telescope: 327-MHz Observations

Ooty Radio Telescope (ORT) consists of a linear phased-array feed consisting of 1056 dipoles, 48 dipoles per each of 22 modules, situated at the focus of an off-axis parabolic reflector (Swarup et al., 1972). The dimensions of the reflector are $\sim$ 500m in the North-South dimension, and 30 m in the East-West, and is on an equatorial mount. The antenna is sensitive to only the N-S polarization, and has a collecting area of $\sim 8000 m^2$. The telescope operates at a fixed center frequency of 327 MHz with a bandwidth of about 12 MHz. The full width at half maximum (FWHM) of the the (N+S) total power and the (NxS) correlation beams in the North-South are $5'.5 sec(\delta)$ and $3'.3 sec(\delta)$ respectively, where δ is the declination of the source. The FWHM is 2° for both the correlated and the total power beams in the East-West direction. For our observations, we have used the central (total power) beam and sometimes an adjacent beam, designated Beam 7 and Beam 5.

The sensitivity of ORT was measured by pointing the telescope toward a calibrator source and determining the increase in the output power with respect to an off-source position. The signal-to-noise measured on a 1-Jy source for ORT on an average is 25, for an integration time of 1 s and a bandwidth of 4 MHz. We quote the measured sensitivity during our observations, to compare it to this standard value.

The pulsar receiver used for our observations was built for the purpose of pulsar searches (Ramkumar et al., 1994). In this set-up, the front end of the receiver consists of a 4-bit sampler (with A/D converters) which samples the incoming intermediate frequency (IF) signal of a total bandwidth 8 MHz at Nyquist rate and feeds this signal into a 512-point FFT engine. The FFT-engine produces 256-point complex spectra which are converted into power spectra. The resultant power spectra are pre-integrated over 0.5 ms or 0.25 ms, defining our sampling interval, and then 1-bit digitized after mean subtraction in each of the spectral channels separately. The digitized data from 256 channels (256 bits per spectrum) are stored on magnetic tapes.

6.3 Search Technique

A general search algorithm for pulsars scans an observed time series in the parameter space of period and DM looking for a periodic, dispersed, pulsed signal significantly above the background of random noise. In this section, we discuss our strategy used to search for pulsations in the direction of Geminga and SAX J1808.8–3658.

In the case of both, Geminga and SAX J1808.8–3658, high energy observations have provided us with a reliable and sufficiently accurate solution for the pulse period and pulse arrival time. Since the distance to the Geminga is known very accurately, and reasonably so in the case of X-ray millisecond pulsar, the expected DM for these pulsars can be estimated. An accurate distance to Geminga is known from the parallax measurements to be 157^{+59}_{-34} pc. For an assumed average electron density of 0.03 per cm^3, the expected value of the DM is $\sim 4.5\, pc/cm^3$. The reported Russian observations of Geminga have yielded a DM close to $3\, pc/cm^3$. The distance to SAX J1808.8–3658 is estimated to be ~ 4 kpc, from which we estimate its DM to be close to $150\, pc/cm^3$. Given the possibly large uncertainties in the assumed electron densities, these DM estimates are treated as only "indicative".

There is one further simplification due to the average pulse-shapes of the two pulsars at high energies: the pulse profiles are more or less sinusoidal. Though one may argue for the radio pulse shapes to be different from the high-energy light-curves, we would like to point out that the radio pulsars with high energy emission, like J0437–4715, B1821–24, Crab, all have high-energy light curves very similar to their radio pulse-shapes (Backer & Trümper, 1999). We believe that the profile of any possible pulsed-radio emission from SAX J1808.8–3658 is well approximated by a single sinusoidal curve (figure 6.4). Geminga is expected to show a broad pulse profile, in fact, all the reported pulse profiles of Geminga at 102 MHz have a very wide pulse ($\sim$ 50% duty cycle), with a possible interpulse emission.

Due to the above two reasons, we employed a simple search strategy for our intended searches. We obtained the fluctuation spectrum of a dedispersed time-series corresponding to an assumed value of DM as a step in our DM-grid search. We selected a window of frequency width ($6f$) around the expected rotational frequency (f_0) of the pulsar, and its second and third harmonics. The position and strength of the maximum in the selected spectral window ($6f$, 26f , & $36f$ around f_0, $2f_0$, & $3f_0$ respectively) were noted for each of the values of DM. This step-wise procedure is outlined below.

- We begin our analysis with a time-frequency matrix of intensities (equivalent to a spectrom-

eter) with a total of 256/512 channels and a time resolution better than one millisecond.

- We step through different values of DM in the range zero – DM, in suitable steps (6DM).
- For each DM, a dedispersed time series is obtained and a fluctuation spectrum is computed.
- For a given DM, we monitor a select window of width $6f$ ($26f$, 36f) around the fundamental frequency (f_0), as well as its immediate two higher harmonics ($2f_0, 3f_0$). This spectral window data is recorded for further analysis. The locations of the maxima within the prescribed range of frequencies and their intensities are noted.
- We change the value of DM to repeat the above step, and note the six values (strengths and locations of the three spectral peaks), along with the full information in the three spectral windows.

For the correct value of DM, the strengths of the fluctuation features corresponding to the pulsar period would be maximum. On either side of the correct DM, the amplitude of the fluctuation features would drop. The position of the peaks corresponding to the pulsar signal will not change for a range of DMs close to the actual DM, and will correspond to the apparent rotational frequency of the pulsar. The rise and fall in the amplitudes of the harmonics around the expected DM and the constancy of their positions are, therefore, treated as the signatures of a pulsed, dispersed signal. We searched for such signatures in our data (see the figures 6.6 and 6.7). However, the spectral positions of peaks selected by the algorithm will happen to be random if the amplitude of the features are not significantly higher than the noise level.

Geminga

The search technique is illustrated for the test pulsar B0950+08 (detected as a strong pulsar in these observations). We show the fluctuation spectrum of a dedispersed time series of this pulsar for a DM (close to its actual value of 2.9701 pc/cm^3) in the figure 6.6. The top panel shows the spectrum up to the 20^{th} harmonic of the pulsar's expected rotational frequency (f_0). Regions of width $\delta f/f \sim 0.001 f_0$ around f_0, $2f_0$, and $3f_0$ were monitored. The location of the peak in each region and its strength were noted for each value of trial DM. The bottom panel shows an expanded spectrum up to twice the expected rotational frequency of the star; note the frequency being plotted is in Hz. A significant feature close to 3.8 Hz is apparent, and was the one picked up by our search algorithm, and was seen over a range of DMs close to $2.97 pc/cm^3$.

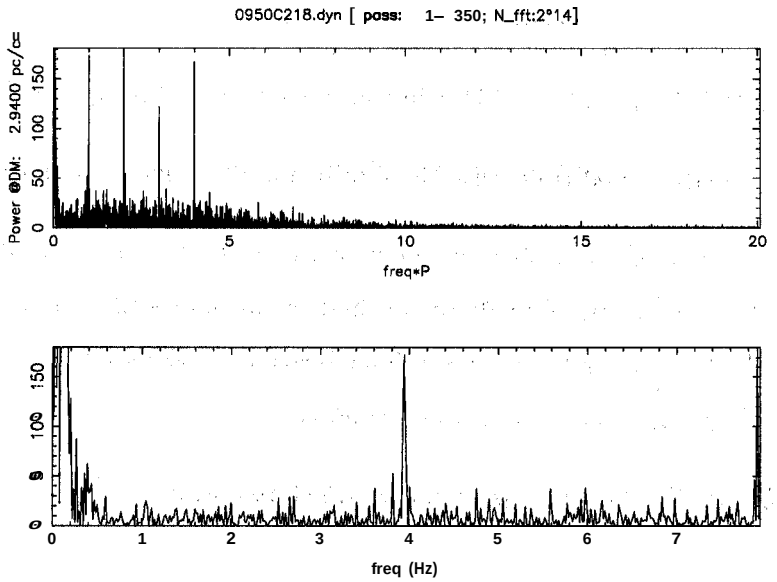

Figure **6.6:** Pulsar B0950+08: The fluctuation spectrum for a dedispersed time series using a trial value of DM (close to the actual value of $2.9701\,pc/cm^3$). The top panel shows the spectrum up to the 20^{th} harmonic of the pulsar's expected rotational frequency. The first four harmonics are clearly visible in the spectrum. Regions of width $6f, 26f, 36f$ around the first three pulsar harmonics were monitored. The bottom panel shows an expanded spectrum up to the twice the expected fundamental frequency of rotation. The scale of frequency on the X-axis is in Hz. A significant feature close to 4 Hz is apparent in this plot, and was the one selected by our search algorithm for monitoring over a range of DMs (see the figure below). The second harmonic is also apparent in the spectrum on the right edge, and is stronger than the fundamental.

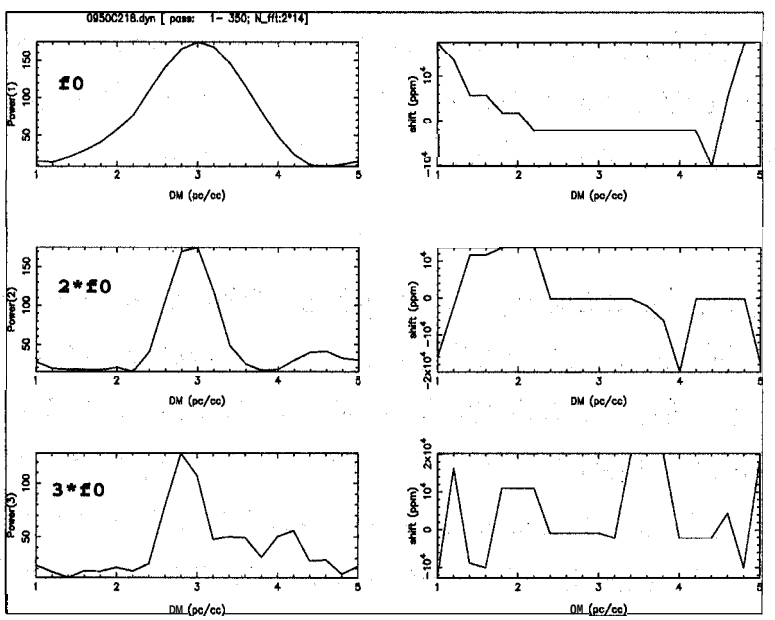

Figure **6.7:** B0950+08: Output of the search algorithm. The power of the peak in a specified range (δf) around the expected fundamental frequency, and similarly powers of the peaks in a range around the second and third harmonics, are plotted on the left as a function of DM assumed during the grid-search. The fundamental frequency is in the top figure, with the second and third harmonics in the bottom (left) figures. The positions of these peaks relative to the value of the expected frequencies are plotted correspondingly on the right (the shifts are denoted in units of parts per million).

In figure 6.7, the fundamental and the two harmonics of the pulsar frequency features peak at $DM = 3.0$, close to its actual value of 2.9701pc/cm^3. The strength of the local maximum (in the prescribed window of frequencies) close to the pulsar fundamental frequency is enhanced when the DM is close to the correct DM (known value of $2.9701\,pc/cm^3$), and the strength of the peak changes significantly with a change in DM of $\gtrsim 0.2\,pc/cm^3$ on either side of the known value of DM. The strength changes by a factor of ~ 10 for a change in DM by $1\,pc/cm^3$. The spectral position of the fundamental picked up by the algorithm (plotted in the top-right panel) remains unchanged in the range of 2 to 4 in DM. The higher harmonics mimic the behavior of the first harmonic, though the range of DM over which the higher harmonics display this behavior is reduced.

We expect a low dispersion measure for Geminga. The reported detections by the Russians groups provide a value of DM close to $3\,pc/cm^3$, with rather large error bars of $\pm 1\,pc/cm^3$. So, we have searched for DM between $0 - 8\,pc/cm^3$. We have also searched for any transient, strong, burst-like emission, or (Crab-like) giant pulses from Geminga. We subdivided our data sets and searched for the possibility of a strong, transient, periodic signal using the strategy above.

SAX J1808.8–3658

We now apply the same technique to the test pulsar for 327-MHz observations, B1937+21. We have used a step of $SDM = 1.0$ in DM for this search. B1937+21 is a distant, millisecond pulsar. We use the available timing model to compute the expected apparent period at epochs of our observations. B1937+21 also displays an interpulse, hence there is enhanced power in the second harmonic of the rotation frequency, *i*.e. $2f_0$.

A narrow window (of width $0.001f_0$) close to the fundamental rotation frequency of B1937+16 and its higher harmonics is plotted in figure 6.8. Strong fluctuation features are apparent in all the panels close to the expected frequencies, and were selected by our search algorithm over a range of DMs close to the known DM. In figure 6.9, the strengths of the chosen fluctuation features display a maximum at $DM \sim 71.0\,pc/cm^3$, close to its actual value (of $71.04\,pc/cm^3$), and they drop to noise level (a factor of $\gtrsim 10$ lower) for a change in DM of $\sim 1\,pc/cm^3$ away from the correct value. The position of the chosen feature close to f_0 (plotted in the top-right panel) remains stable over a DM change of $< 2\,pc/cm^3$, whereas the position of the maximum close to first harmonic remains the same over a larger range of DMs. For SAX J1808.8–3658, we use the available results from X-ray pulse timing to derive the change in the pulse period as the phase of the pulsar in the binary orbit changed over different observations. Using these estimates, all the time series were resampled suitably such that the spectra were appropriately scaled before examination, and were

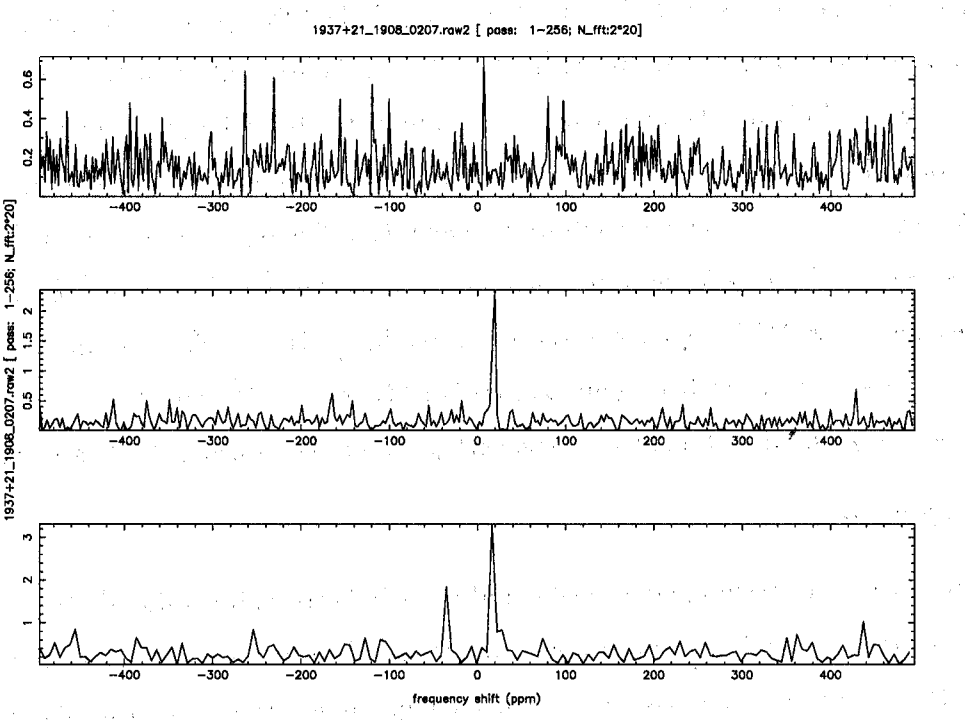

Figure 6.8: The test case, B1937+21: The fluctuation spectrum for a dedispersed time series using a trial value of DM (close to the actual value of $71.04 pc/cm^3$). The bottom-most panel shows a small portion of the pulsar spectrum close to the rotational frequency ($\sim$ 642 Hz), whereas the other panels show the same in the case of its higher harmonics. The locations of the computed (expected) frequencies are at the center of all three panels. Spectral frequencies are represented in terms of their distance from center in parts per million (ppm) on the X-axis. A significant feature is apparent in the bottom panel, and was selected by our search algorithm for monitoring over a range of DMs (see figure 6.9). The feature in the top panel (corresponding to the third harmonic) does not appear at the same location as that of the other two, and is consistent with it being a chance peak due to noise.

The locations of features corresponding to the fundamental and its second harmonic are shifted from zero. Such a shift is due to a possible deviation in the sampling clock frequency from its assumed value. This shift was used in our analysis to calibrate the frequency of the sampling clock.

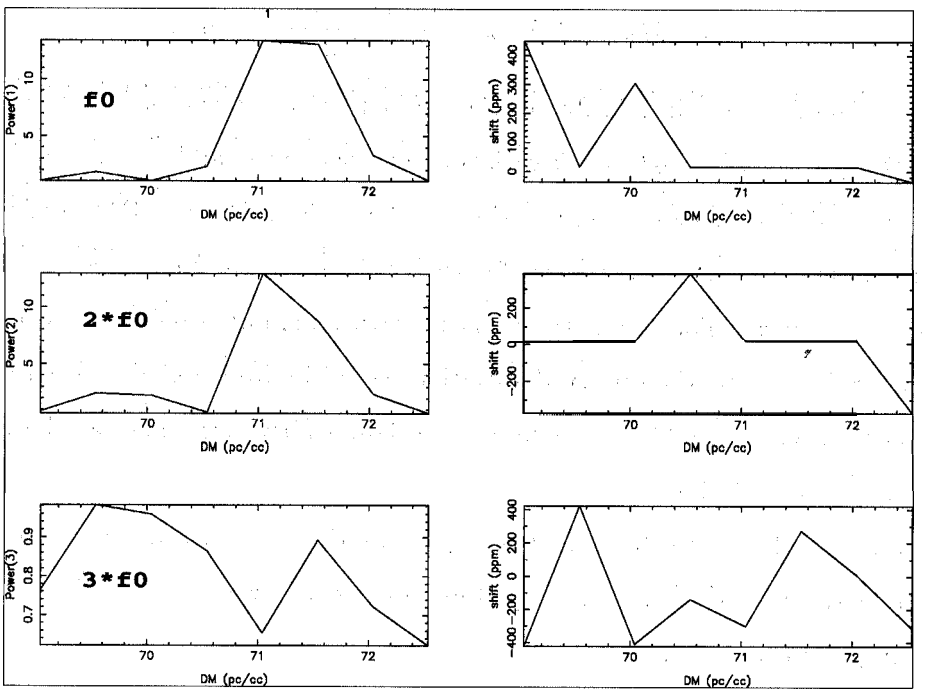

Figure **6.9:** The test case, B1937+21: Output of the search algorithm. The strength of the peak in a specified range (Sf) around the expected fundamental frequency, and similarly powers of the peaks in a range around the second and third harmonics, are plotted on the left **as** a function of DM assumed during the grid-search. The fundamental frequency is in the top figure, with second and third harmonics in bottom (left) figures. The positions of these peaks relative to the value of the expected frequencies are plotted correspondingly on the right (the shifts are denoted in units of parts per million). Note that the steps in DM are of size 1, and the power in the fundamental feature has increased by a factor of $\gtrsim$ **10** at the correct DM of the pulsar as compared to the power corresponding to earlier and later DMs.

also combined to improve the detectability of the spectral features.

If some quasi-eclipsing phenomenon involving the companion star (such as stellar wind) was responsible for the observed faint X-ray dips (2%) in the case of SAX J1808.8–3658 (Chakrabarty & Morgan, 1998), such an eclipsing body can cause a deeper apparent radio eclipse due to enhanced dispersion and scattering. We have tried to account for such a possibility of some DM variation over the orbital phase of the pulsar using a simple model for such a variation given by

$$\delta DM_{\Phi} = \delta DM_{max} \left(\frac{1 - cos(\Phi - 270^{\circ})}{2} \right)^{\gamma}, \tag{6.6}$$

where δDM_{Φ} is the variation in DM due to the companion at a given phase in the binary orbit, Φ in degrees, δDM_{max} is the peak-to-peak variation over one cycle, and y is a constant, a power law index to allow for higher harmonic contributions of the basic single-tone DM modulation. Modeled in this form, the DM variation maximizes for the phase when the binary companion eclipses our line-of-sight to the pulsar. For $y = 1$, the variation takes a simple single-tone form. In a real case of an eclipsing radio pulsar, the observed variations could be over a shorter fraction of the binary orbit (y larger than 1), and δDM_{max} could also be significantly large, making the variation appear more like a pulse-like variation.

We have searched for values of δDM_{max} as large as 9, and that of the non-linearity y up to 6. The power spectra for each of the 10/20 minute sessions were examined separately as well as after combining them together.

6.4 Results

6.4.1 Geminga

Resultant spectra from our observations on all six observations are shown in figures 6.10 and 6.11. The spectra do not show any significant signatures (figure 6.7) of an apparent pulsation from Geminga, with a periodicity of $\sim$ 237 ms in the range of DMs searched. We have also combined power spectra from all six data sets, and looked for any signatures of pulsations. The analysis yielded a null result again, see figure 6.12. Our results put an upper limit on the average pulsed flux from Geminga, using a single observation is, $\sim$ 350 mJy (30). The combined spectra yield an upper limit of $\sim$ 150 mJy (30).

Our collaborators reported strong pulsations at $\sim$ 111 MHz on the 5^{th} and 6^{th} of February, 1999, with the average profile displaying a detectable interpulse. In these observations 4 channels of width 20 kHz each were used, and single-pulse sequences with a time resolution of $\sim$ 7.68 ms were generated. Short sequences, of typically 12-50 pulsar periods ($\sim 5 - 20$ s), were used to fold

and detect any signatures of a pulsed signal. The pulsar was detected on the following days as well, but appeared weaker.

Considering the strong pulsed signal reported at 111 MHz, we searched our data obtained on the 5^{th} February, 1999, for a periodicity in shorter sections of the data set. The data on 6^{th} February were affected by interference, and hence not very useful. We could not confirm any periodicity even in short sections of the data observed on 5^{th} February. Figure 6.12 shows the results for our best possible section of this data where a tentative suggestion of a signal could be made. However, the relevant fluctuation feature in the spectrum has a low significance. We folded this section of the time series at twice the period of the fluctuation feature, and do not see any apparent pulse (see figure 6.13). Hence, we would like to stress, that we do ***not*** confirm any periodicity in the data from this analysis, though it remains an interesting possibility. We need more attempts with similar type of observations and analysis to confirm this tentative feature in our spectra.

If confirmed, the dispersion measure is, $\sim 3.2 pc/cm^3$. The average flux is $\sim 1 Jy$ for the detection over this short duration of $\sim$ 75 seconds. Such an emission would then imply pulses of energy $\gtrsim$ 10 times the average pulse energy expected based on the reported values of Geminga radio flux at 100 MHz.

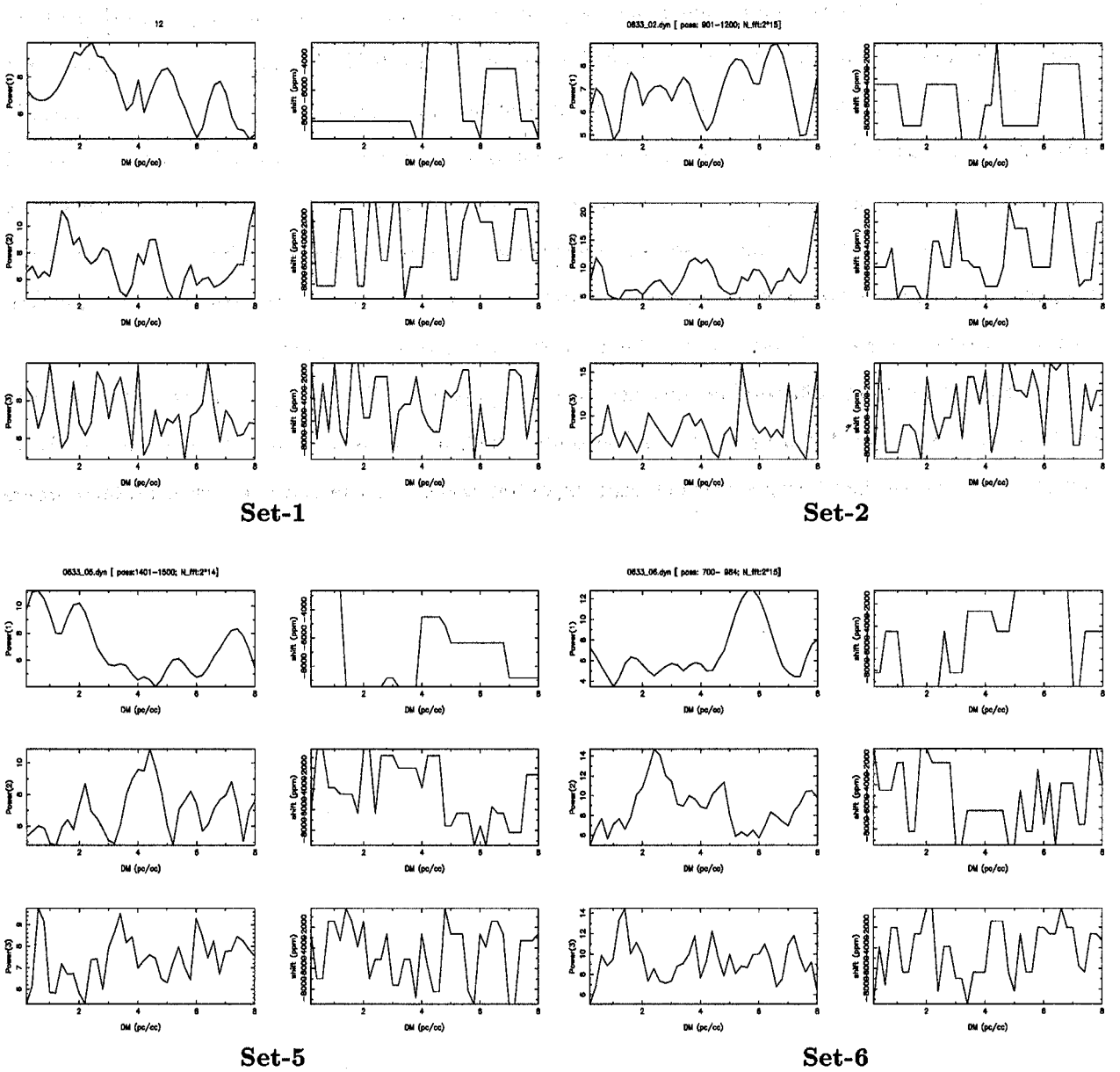

Figure 6.10: Geminga: result of our search in individual data sets— we look for signatures of the type shown in figure 6.7. No significant features were found in this data set in the range of DMs searched, let alone near the expected value of 3.

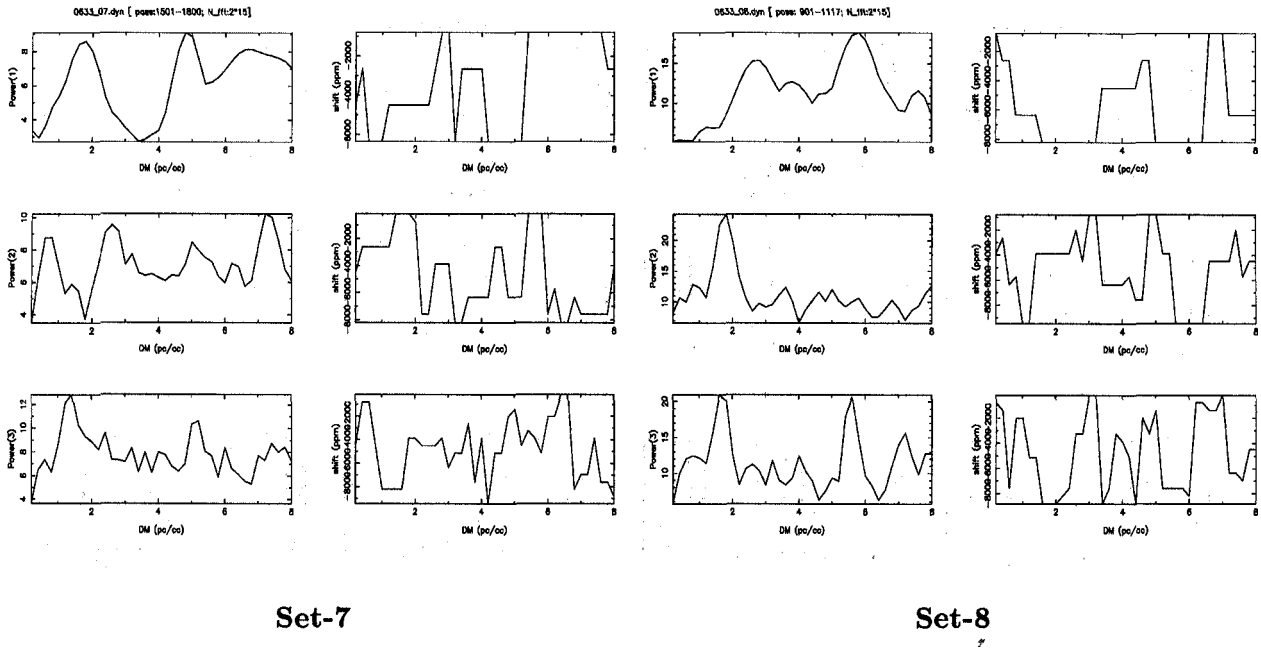

Figure *6.11:* Geminga: result of our search in individual data sets— we look for signatures of the type shown in figure *6.7.* No significant features were found in this data set in the range of DMs searched, let alone near the expected value of **3.**

6.4.2 SAX J1808.8–3658

We have searched for a signature of radio pulsation after scanning over a wide range of DMs $(0 - 250 pc/cm^3)$. Our search using power spectra from *6* individual data sets are presented in the figures *6.14* and *6.15.* We look for a signature of the type shown in figure *6.9.* No significant pulsar-like signal was apparent in any individual data set, each of a total of *10* min in duration.

As a next step, we combined results from all the data sets, where we made use of eq. *6.6* with varying values of δDM_{max} and γ. We added power spectra from all the data sets for each of the combinations. Figure *6.16* shows the output of such an analysis. No significant pulsed radio emission was evident.

The non-detections in this analysis imply an upper limit of ~ 2.5 mJy (3σ) for the average radio emission from this object using an individual data set. **A** better upper limit for flux density using the combined spectra is $\sim 0.8\ mJy$.

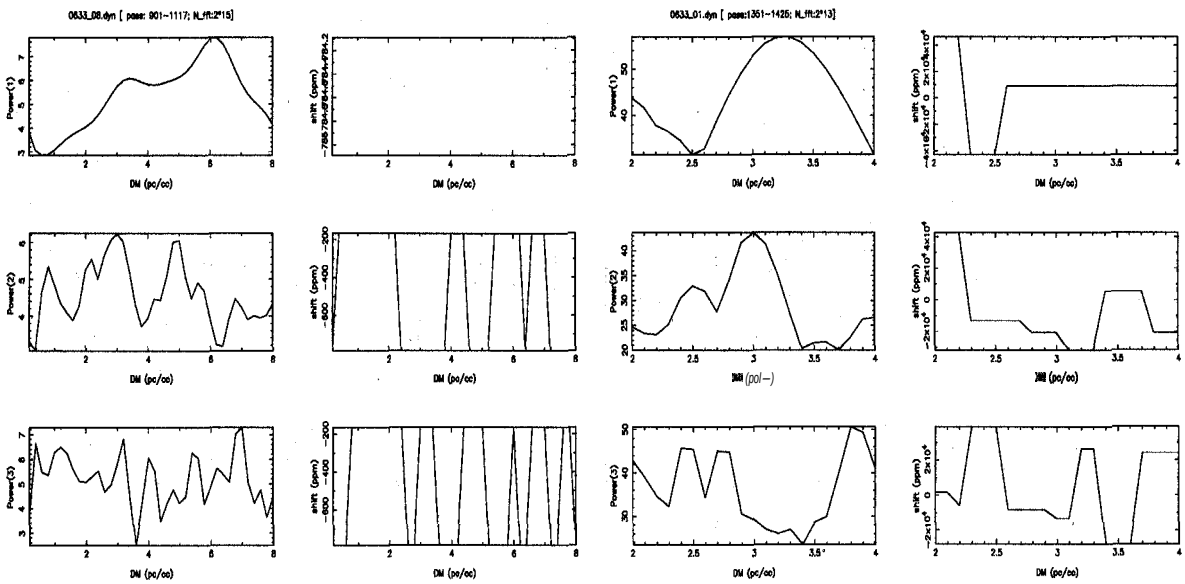

Results of **all** data combined. **A** tentative signature.

Figure **6.12: Left** Resultant spectra after combining individual spectra from six observations shown in the figures **6.10** and **6.11.** There is no signature of a pulse in the combined data. **Right A** tentative result using shorter sequences of the data. The plot was created using a shorter sequence from our observed data on 5^{th} February, **1999. A** minor increase in the power at the fundamental frequency, and also at the second harmonic, close to a DM of $3\,pc/cm^3$ was apparent.

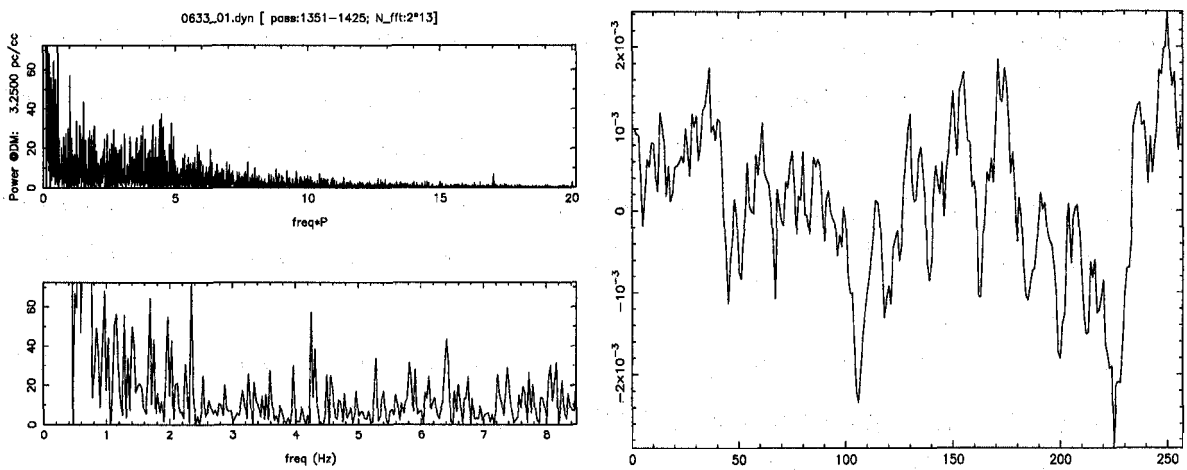

Figure **6.13: Left:** The plot shows the fluctuation spectrum for the same stretch of data as in the tentative feature mentioned in figure **6.12.** We have used some **300** pulses for the analysis shown. The spectrum shows the low significance of the fundamental feature in the fluctuation spectrum. We folded this section of the time series at twice the period as that of the implied fluctuation feature in the spectrum, shown on the **right.** No pulse feature is apparent in the folded data.

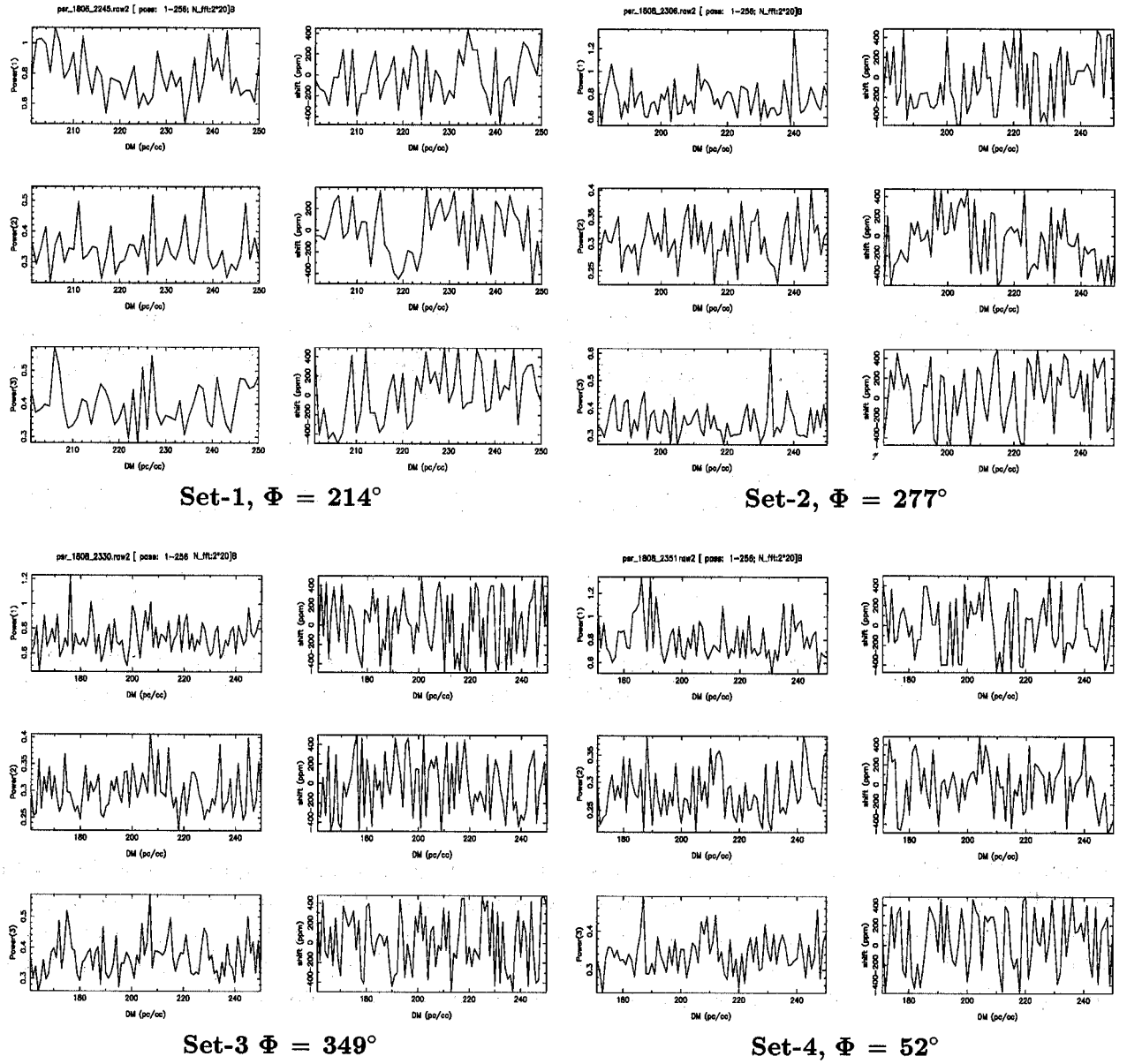

Figure **6.14:** SAX J1808.8–3658: Search results from power spectra computed from individual data sets. The orbital phase of the pulsar at the beginning of the acquisition of each data set is noted below the respective figures. The last two data sets shown above have a time constant of **0.25** ms, whereas all other observations have a time constant of **0.5** ms. No significant 'pulsar-like' features were found (see figure **6.9** for an example of a signature of 'detected' pulsar).

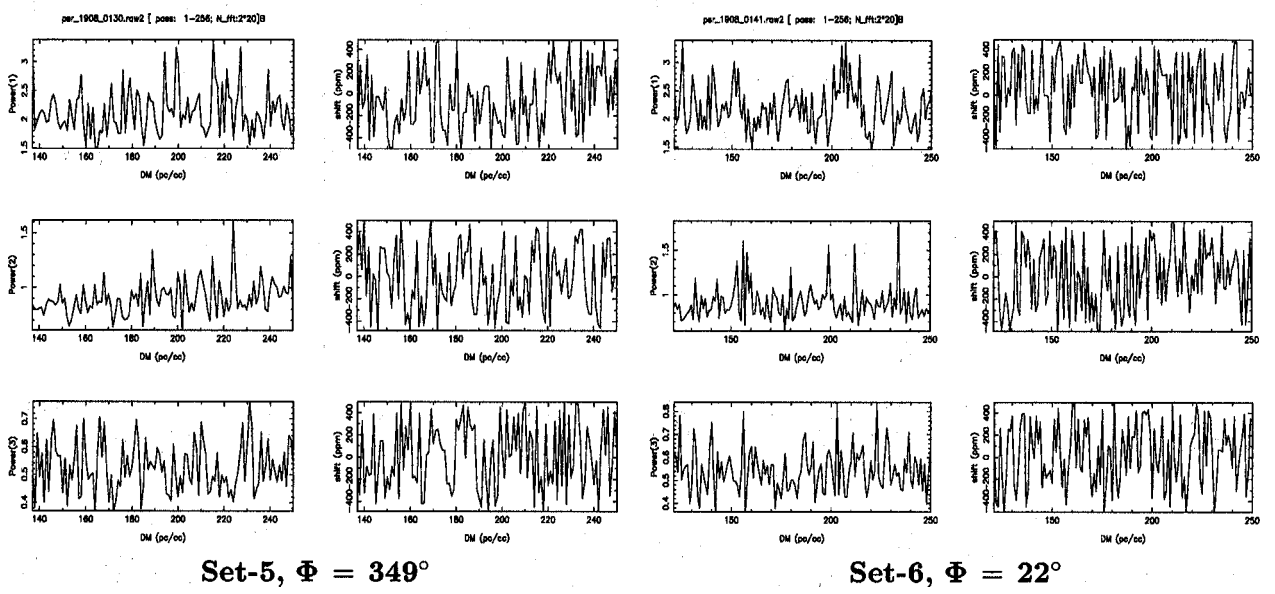

Figure 6.15: SAX J1808.8–3658: Search results from power spectra computed from individual data sets. The orbital phase of the pulsar at the beginning of the acquisition of each data set is noted below the respective figures. The last two data sets shown above have a time constant of 0.25 ms, whereas all other observations have a time constant of 0.5 ms. No significant 'pulsar-like' features were found (see figure 6.9 for an example of a signature of 'detected' pulsar).

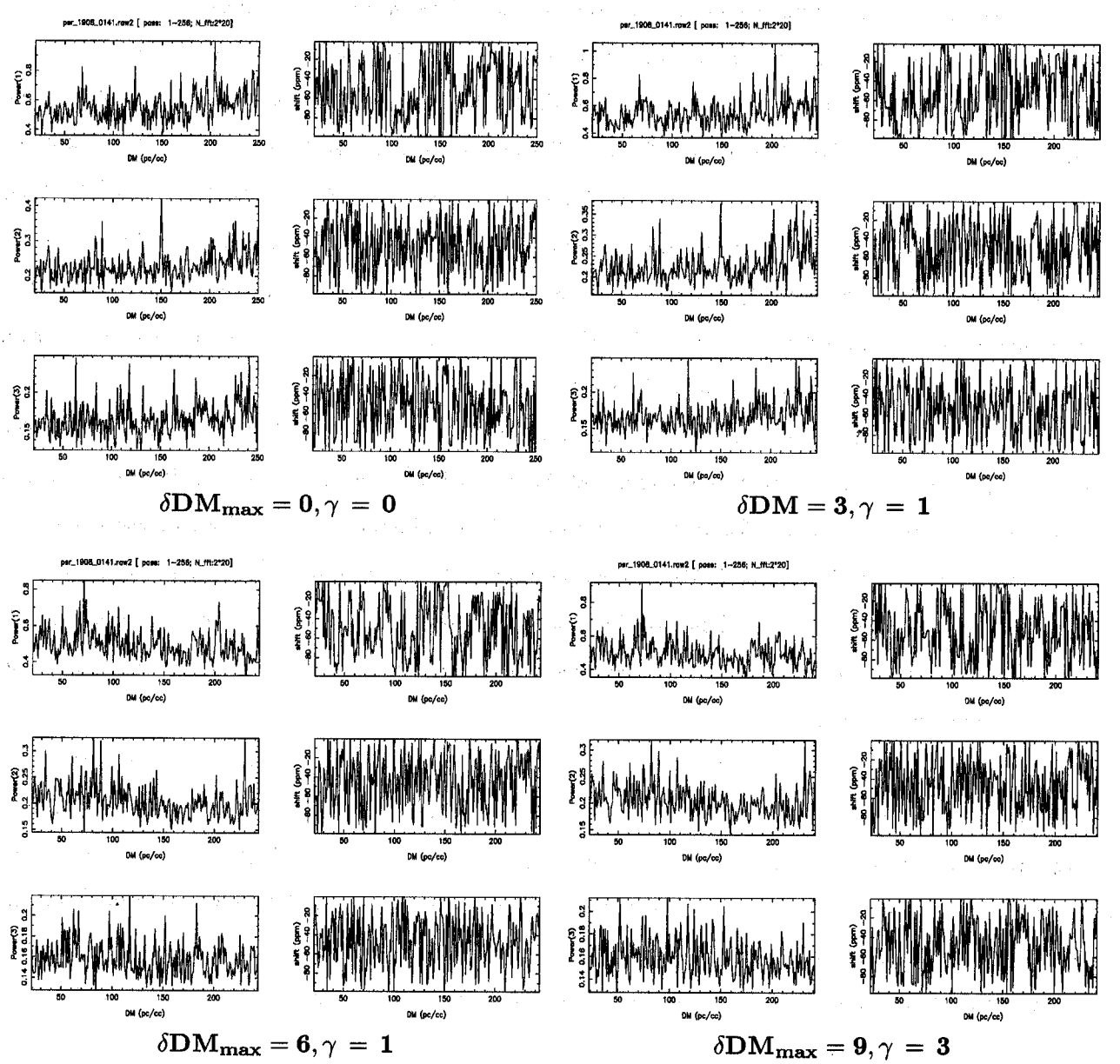

Figure 6.16: SAX J1808.8–3658: Searching the combined power spectra after correcting for a possible DM variation due to ionized material in the companion's wind. The top-left plot shows the results when no variation in dispersion measure with orbital phase was considered.

6.5 Discussion and summary

In this chapter, we discussed our attempts to detect pulsed radio emission from two high-energy pulsars, Geminga and SAX J1808.8–3658.

The gamma-ray pulsar Geminga attracted the attention of astronomers recently, with the reported detection of its pulsed radio emission at 102 MHz by three Russian groups. Since Geminga, one of the brightest Gamma-ray sources in the sky, is the only known gamma-ray pulsar that has not been detected in the other parts of the radio spectrum, confirming its pulsed radio emission and determining the reasons for its radio weakness may be essential to understand the relationship between a pulsar's gamma-ray and radio emission. Since the reported discovery, none of the other groups which observed Geminga for pulsed radio emission could confirm the Russian claim of detection (this also included a search at 35 MHz using the GEETEE — Deshpande, Ramachandran, & Indrani, 1998) at a frequency other than 100 MHz.

These negative results meant that the pulsar was either too weak to be detectable at the frequency of observation (detectable only at 102 MHz), or is a transient source. Refractive scintillation could also make its detection difficult at times. We conducted near-simultaneous observations of Geminga at 111 MHz and 34.5 MHz at Puschino and Gauribidanur. With such a data set, we aimed to confirm the correspondence of detection in Puschino and GEETEE data. If the pulsar was an intermittent source of a few intense pulses (*e.g.* giant pulses from Crab), we could confirm such a behavior in our data set.

The initial analysis of Puschino data indicated a significant pulsed emission, with a detectable interpulse. However, there was no detection of a pulse in 35-MHz data on the corresponding days. Our estimated upper limit on the average flux of Geminga at 35 MHz is ~ 350 mJy (3σ) using data obtained on a single day. Shorter intervals of data were searched for a possible intermittent emission, with a null result. Such a null result meant that any giant pulses, if possible, were below a flux limit of 1 Jy, and did not occur over a duration of 70 seconds, that was analysed in detail.

The transient nature of Geminga, or propagation effects, are therefore less likely to contribute dominantly to the non-detection of pulsed radiation at 34.5 MHz. One needs to invoke, then, unreasonably steep spectral roll-offs above and below 100 MHz to explain the non-detection at frequencies other than ~ 100 MHz.

A likely reason for such a steep spectrum above 100 MHz would be geometric: our line-of-sight may cut the emission cone of Geminga at its edge when observed at 100 MHz. Then, we are

more likely to miss the emission entirely, if the cone becomes narrower at higher frequencies. This scenario can be consistent with upper limits obtained for pulsed emission in decameter band, only if the flux densities at 102 MHz were grossly overestimated.

The recent detection of coherent X-ray pulsations with a millisecond period from a suspected LMXB system appears to confirm the evolutionary link between the low mass X-ray binaries (LMXBs) and millisecond pulsars (MSPs). An exciting possibility is that SAX 51808.8–3658 will, at some point, turn on as a radio pulsar, thus producing pulsed-radio emission characteristic of MSPs. We searched during the X-ray quiescence state of this system, for possible radio pulsation at 327 MHz using the Ooty Radio Telescope.

This search was tuned for the known binary system parameters, where the effects of binary acceleration on pulsar periodicity, and some possible extra dispersion variations due to the passage of the radio pulse through a possibly extended wind from the companion, were taken into account. Our search was aimed at detecting a near-sinusoidal signal, and we searched up to a maximum DM of $250\,pc/cm^3$.

We did not detect any pulsed radio emission from the system at 327 MHz. The upper limit for radio emission from one single observation of 10 minutes duration, is $\sim 2.5\,\mathrm{mJy}$ (30). We combined power spectra from consecutive observations. A possibility of a variable DM due to interaction with the binary wind in SAX 51808.8–3658 was considered. Using a simple model for such a change in DM, we combined suitably scaled power spectra from consecutive observations of 10 minutes each. Even in this case, we did not detect any pulsed radio emission. The upper limit on the flux density of possible pulsed radio emission, based on our search, is $\sim 0.8\,\mathrm{mJy}$ (30).

Recent observations suggest a possible interaction between radio emission and accreted matter. It is anticipated that the system will emerge as an MSP, though strong absorption and interaction with the stellar wind are likely. Sensitive searches for pulsations should, therefore, continue.

Chapter 7

Conclusions

We now conclude this thesis with chapter-wise summaries of our results.

In **chapter** 3, we presented the average properties of 8 pulsars at 34.5 **MHz** using our observations with the Gauribidanur array. We based our sample selection on the catalog of known pulsars (Taylor, Manchester,& Lyne, 1993), wherein the properties of pulsars known from the meter wavelength observations were available. We estimated the expected pulsar flux densities in our band for the candidates using their available properties at meter wavelengths and the short-list consisted of pulsars that could be detected with a 1000 s integration. The sample contained a total of ~ 40 pulsars. Pulsar B0943+10 was included in this list, though it was not selected by our criterion. The selected sample was monitored in the summer of 1997, when observations in the direction of every pulsar in the list were made for an effective duration of $\sim$20 minutes. Some of the strong pulsars were observed again in 1999. The acquired data were analysed, and a total of 8 pulsars were detected. We have presented the average-pulse profiles obtained in these cases. The relevant inferred parameters associated with the average profiles observed are also presented.

Average profiles at 34.5 **MHz** show an increase in the pulse width, and component separation in the case of 'double' profiles, when compared to those at higher frequencies. The profile widths are known to increase at lower frequencies following a power law. Comparing with higher frequency results of Slee et al., 1987, we find the power law index to be steeper than $\nu^{-0.3}$. The average profiles containing two components may also display asymmetry in two aspects: the intensities of the two components may differ, and/or their locations around the central fiducial point, defined as the location where the pulsed power drops to noise level in between the components, may be asymmetric. Such asymmetries, with a varying degree of significance, were observed in four cases of double profiles in our sample. Such asymmetries can originate from a slight non-circularity of the polar cap being sampled by symmetric locus of our sightline, a scenario suggested by Arendt

& Eilek (2000).

Our time resolution allows us to study the intrinsic modulations due to subpulse phenomena, which occur on milli second time scales or higher. Information about the strength of such modulations can be obtained by measuring modulation index m at every pulse longitude to study the depth of modulation across the pulse profile. We have computed the modulation index profiles as a function of pulse longitude for seven pulsars, and these results are presented. The modulation indices are seen to vary across longitude, and are, therefore, most likely due to an underlying "intrinsic" fluctuation phenomena.

Radio-flux density spectra of many pulsars have been studied based on the reported flux measurements at various radio frequencies (Malofeev *et al.*, 1994). Typically, pulsar flux densities show a decrease with increasing frequencies and follow a steep power law, $S_\nu \propto \nu^{-\alpha}$ $(-1 > a > -3.0)$, and display a turnover typically close to 100 MHz, below which flux densities have a more or less flat spectrum or even a decline. We have presented the flux-density estimates from our observations at 34.5 MHz. These estimates were obtained by fitting Gaussian profiles to the pulsar profiles. The area under the fitted profile was calibrated to get the average-pulse energy. Our measurements are consistent with the published spectra based on earlier measurements.

Estimates of flux density are prone to errors due to source variability, apart from systematic calibration errors. We have discussed two specific cases, *viz*, the scintillation effects and the intrinsic variability.

In **chapter** 4, we discussed the conventional tools to study the various types of single-pulse fluctuation phenomena, which include the fluctuation spectra and correlation analysis. We studied eight bright pulsars in our observed sample for their single-pulse properties.

A very powerful and conventional tool, 'longitude resolved fluctuation spectra' (lrf-spectra; Backer, 1973), brings out any systematic of single-pulse fluctuations as a function of time (pulse number) and pulse longitude much more clearly than possible in the time domain. However, such spectra have a serious drawback of aliasing. Such an aliasing hinders determination of the exact frequency of a spectral feature and any possible harmonic relationship between various features.

To address the issue of aliasing in spectra, we follow the approach taken by Deshpande & Rankin (1999: DRa, 2001:paper-I). We Fourier transform the entire continuous pulse sequence, which can be reconstructed (from the "gated" version) by using the available samples on within the pulse window, and filling the unsampled longitude (off-pulse) region with zeros. We choose to present the raw fluctuation spectrum in another manner, where we stack the successive sections of the spectrum of width $(1/P_1)$. We refer to this spectral representation an "harmonic-resolved

fluctuation spectrum", or an HRF-spectrum.

Such an hrf-spectrum does not have the same limitations of sampling as does an lrf-spectrum. An **hrf-spectrum** can further distinguish between the two types of pulse modulations encountered, *vix.* amplitude- and phase-modulations. However, an hrf-spectrum does not resolve the issue of aliasing entirely on its own. One has to invoke further constraints to understand any possible aliasing of features. Various issues regarding lrf- and hrf-spectra were discussed in sections 4.2.1 and 4.2.2.

We have presented fluctuation-spectral analyses of 8 bright pulsars in this chapter, and discussed the individual cases. It is found, in general, that pulsars show significant fluctuation even at these low frequencies. Fluctuation power (as a function of the total) varies from pulsar to pulsar, and in some pulse sequences the entire fluctuation power was observed to belong to the associated primary modulation. The fluctuation spectral features in the case of known 'drifters', B0943+10, B2016+28, and B1919+21, are sharp. The feature in the lrf-spectrum of B0943+10 remains partly unresolved even after using 512 pulses in the transform, consistent with the spectra at 430 and 100 MHz. The high Q-value of the feature shows that the drift process giving rise to modulation is remarkably stable even at 35 MHz, though the Q-value was certainly less in our data compared to that in meter-wavelength data.

The frequencies of the primary modulation in our spectra show a reasonable match with those observed in the meter-wavelength fluctuation spectra. The frequency of the modulation could vary slightly over different data sets, typically by a few percent of the mean value. The average frequency of the modulation remains unchanged with frequency, however, *irrespective* of whether the feature is broad or narrow. This is to say, that the frequency is unchanged even in the cases where the modulation appears to be erratic and has thus produced broad features in the spectra.

The lrf- and hrf-spectra are best suited to study periodic modulations, and in particular the drifting-subpulse phenomenon. But, for some cases, where no apparent drift is observed, and/or where the amplitude modulation may not very periodic, useful information can be sought through suitable time-domain analysis. To investigate a mutual correspondence between the fluctuations at different longitudes, a cross-correlation analysis of intensity fluctuations at different pulse longitudes was performed. In section 4.3, we detailed issues related to cross-correlation maps over the entire pulse region (2-D) with a fixed pulse-number delay. We have presented the relevant correlation analysis of the data on all pulsars discussed in the previous section. An asymmetry in the correlation maps for one- and two-pulse delays in the case of B0834+06 and B1133+16 offers a possible solution to the drift direction in the case of these two pulsars.

In **chapter** 5, we presented our analysis of the single-pulse fluctuations observed in the decametric emission of pulsars B0943+10 and B0834+06 in detail and tried to understand the observed diverse single-pulse fluctuation properties in terms of polar emission patterns and their temporal behavior. We compared our observations with the general picture of radio emission patterns and subpulse modulation elaborated theoretically by Ruderman & Sutherland (1975) and to the higher frequency observational results of Deshpande & Rankin (DRa and paper-I).

We described the theoretical picture suggested by Ruderman & Sutherland in the beginning. We studied the fluctuation features of the two pulsars in detail. The technique of 'Cartographic Transform', where every sample from each single pulse is uniquely mapped onto the polar region of the pulsar, provides new means of studying underlying emission patterns using single-pulse phenomena. We discussed the various issues related to this technique and used it to obtain polar emission maps for these two pulsars.

Although the signal-to-noise ratio in these observations was insufficient to detect individual pulses, we showed that an estimation of the average fluctuation behavior can still be made reliably, if the magnitude of fluctuations is high enough to be detected in the data set as a whole. There is an advantage in using a long pulse sequence only if the modulation features are relatively stable over the relevant integration time scales, as in the present case.

In the case of **B0943+10**, our observations lead to the conclusion that a system of 20 sub-beams, rotating around the magnetic axis of the star with a circulation time $\hat{P}_3$ of about 37 P_1 is responsible for the observed stable subpulse-modulation behavior. Compared with the higher frequency maps, the 35-MHz maps sample the subbeams much more completely in their radial extent However, the 35-MHz subbeams, on the whole, show much less uniformity in their positions and intensities. At both, 35 MHz and the higher frequencies, the intensities of individual subbearns fluctuate, maintaining a stable brightness only for a few circulation times. The stability time scales of the entire pattern appear roughly comparable between 35 MHz and 430 MHz.

Since the particle plasma responsible for the pulsar emission originates close to 'acceleration' zone (which is considered to be located near the magnetic polar cap), whereas the conversion to radio emission occurs at a height of several hundred kilometers above the stellar surface, we are led to conclude that the polar cap is connected to the region of emission via a set of 'emission columns'. This picture is further supported by the very similar emission patterns observed at 35 MHz and 430 MHz—emitted, presumably, at significantly different altitudes in the star's magnetosphere.

We, detect a weak connecting bridge between the two components of the pulse, which is as strong as 20% in one pulse sequence (set-2), and is much weaker in the other (set-1). There

is a little or no fluctuation power observed under this component. We would like to argue that it shares a common origin with the non-fluctuating 'base' component observed at 430 MHz. Such a component may be associated with a much reduced contribution from a possibly bright central 'core' component and deserves further study. Among a total of 6 sets at 35 MHz, we find only one sequence exhibiting a 'Q'-mode behavior—that is, with both the average profile and fluctuation spectra displaying clear deviations from 'B'-mode properties. This predominant 'B'-mode character of the decametric emission in our observations as well as in the earlier observations of Deshpande & Radhakrishnan (1994) is in significant contrast with the trend at higher frequencies where both the 'B' and 'Q' modes may occur with similar frequency of occurrence (Suleymanova et *al.*1998).

B0834+06 is the only other pulsar, apart from B0943+10, for which we could estimate the circulation time of the polar emission pattern reliably using the fluctuation properties and its viewing geometry. This estimation is based solely on the decameter observations! We have made polar emission maps from our data at 34.5 MHz using the estimated $\hat{P}_3$ and drift direction and those were presented in the earlier section. In carrying out this estimation we followed a somewhat general strategy for the estimation of the circulation time of the polar emission pattern. This approach, mentioned below, could be adopted in other cases as well.

We studied the fluctuation modulations of this pulsar. The modulation under the pulse displays a time delay between the two components of the profile. We argued that the amplitude fluctuations associated with each of the two components occur due to the 'passage' of the same emission entity as the entire polar emission pattern revolves steadily around pulsar's magnetic axis. This understanding then allows us to scale the time delay associated with a component separation of some $\delta\zeta$ in magnetic longitude (corresponding to the profile component separation of $\delta\varphi$), thus providing the initial guess for the circulation time. We searched our fluctuation spectra for slow modulation features with frequencies close to this 'guess' of circulation time. We further carried out a search to refine the viewing geometry and other parameters of transform using the inverse of "Cartographic Transform". This method yielded a refined determination of the circulation time and drift direction of the pattern relative to the pulsar rotation, both so crucial for our mapping technique.

Here too, a system of discrete subbeams in steady rotation along the magnetic axis was found responsible for the observed single-pulse fluctuations. The emission beams in the case of B0834+06 are discrete, but they are **not** uniformly spaced along the hollow cone of emission and they all differ from each other in their appearance. The subbeams appear broader in radial cross-section, with $\Delta\rho/\rho \gtrsim 25\%$, and seem to fluctuate around their average position and intensity more

than what was observed in the case of B0943+10.

The increased jitters in the subbeam position could result in the low Q-value of the observer fluctuation features. Also, it was not possible to account for the null pulses, which could further reduce the modulation feature's Q.

We also made maps from successiye subsections of the pulse sequence and viewed them in a 'movie'-like fashion. For all the three data sets of B0943+10 discussed, it was noticed that only a few subbeams (different ones at different times) usually dominated in intensity over a few circulation times. Overall, the brightness of a given subbeam was observed to fluctuate by up to about a factor of 4 over the length of the sequence. Given the above, it is tempting to suggest that (a) an inhibition of emission (or the underlying sparks) occurs over the rest of the polar cap due to the active subbeams, or (b) A critical combination of parameters required for stable, uniform subbeams.

It is important to note, that that pulsar B0834+06 is different from B0943+10 in its physical parameters, the viewing geometry, as well as the nature of the apparent modulation due to drift. The single-pulse fluctuations in this case are general modulation of component amplitudes, unlike the stable 'drift' patterns observed in the case of B0943+10. Even such a general amplitude modulation appears to be related to a well-defined rotating pattern in the polar emission region. This further supports our view that a set of discrete subbeams of emission and their apparent circulation, as envisioned in R&S, results in the single-pulse fluctuations observed. The apparent nature of the modulation is a combination of the pulsar parameters and the observer's viewing geometry.

Overall, our observations of B0943+10 and B0834+06 agrees remarkably with the picture of a steady system of discrete emission subbeams in an apparent circulation around the magnetic axis. This cartoon has a remarkable overlap with the R&S model. When we compare the results for the two pulsars, the observed value of the circulation time of B0834+06 is considerably smaller than that expected from the model.

In **chapter** 6, we discussed our attempts to detect pulsed radio emission from two high-energy pulsars, Geminga and SAX J1808.8–3658.

The gamma-ray pulsar Geminga attracted the attention of astronomers recently, with the reported detection of its pulsed radio emission at 102 MHz by three Russian groups. Since Geminga, one of the brightest Gamma-ray sources in the sky, is the only known gamma-ray pulsar that has not been detected in the other parts of the radio spectrum,confirming its pulsed radio emission and determining the reasons for its radio weakness may be essential to understand the relationship

between a pulsar's gamma-ray and radio emission. Since the reported discovery, none of the other groups which observed Geminga for pulsed radio emission could confirm the Russian claim of detection (this also included a search at 35 MHz using the GEETEE — Deshpande, Ramachandran, & Indrani, 1998) at a frequency other than 100 MHz.

These negative results meant that the pulsar was either too weak to be detectable at the frequency of observation (detectable only at 102 MHz), or is a transient source. Refractive scintillation could also make its detection difficult at times. We conducted near-simultaneous observations of Geminga at 111 MHz and 34.5 MHz at Puschino and Gauribidanur. With such a data set, we aimed to confirm the correspondence of detection in Puschino and GEETEE data. If the pulsar was an intermittent source of a few intense pulses (*e.g.* giant pulses from Crab), we could confirm such a behavior in our data set.

The initial analysis of Puschino data indicated a significant pulsed emission, with a detectable interpulse. However, there was no detection of a pulse in 35-MHz data on the corresponding days. Our estimated upper limit on the average flux of Geminga at 35 MHz is ~ 350 mJy (3σ) using data obtained on a single day. Shorter intervals of data were searched for a possible intermittent emission, with a null result. Such a null result meant that any giant pulses, if possible, were below a flux limit of 1 Jy, and did not occur over a duration of 70 seconds, that was analysed in detail.

The transient nature of Geminga, or propagation effects, are therefore less likely to contribute dominantly to the non-detection of pulsed radiation at 34.5 MHz. One needs to invoke, then, unreasonably steep spectral roll-offs above and below 100 MHz to explain the non-detection at frequencies other than ~ 100 MHz.

A likely reason for such a steep spectrum above 100 MHz would be geometric: our line-of-sight may cut the emission cone of Geminga at its edge when observed at 100 MHz. Then, we are more likely to miss the emission entirely, if the cone becomes narrower at higher frequencies. This scenario can be consistent with upper limits obtained for pulsed emission in decameter band, only if the flux densities at 102 MHz were grossly overestimated.

The recent detection of coherent X-ray pulsations with a millisecond period from a suspected LMXB system appears to confirm the evolutionary link between the low mass X-ray binaries (LMXBs) and millisecond pulsars (MSPs). An exciting possibility is that SAX J1808.8–3658 will, at some point, turn on as a radio pulsar, thus producing pulsed-radio emission characteristic of MSPs. We searched during the X-ray quiescence state of this system, for possible radio pulsation at 327 MHz using the Ooty Radio Telescope.

This search was tuned for the known binary system parameters, where the effects of binary acceleration on pulsar periodicity, and some possible extra dispersion variations due to the passage of the radio pulse through a possibly extended wind from the companion, were taken into account. Our search was aimed at detecting a near-sinusoidal signal, and we searched up to a maximum DM of $250\,pc/cm^3$.

We did not detect any pulsed radio emission from the system at 327 MHz. The upper limit for radio emission from one single observation of 10 minutes duration, is $\sim 2.5\,\mathrm{mJy}\ (3\sigma)$. We combined power spectra from consecutive observations. A possibility of a variable DM due to interaction with the binary wind in SAX J1808.8–3658 was considered. Using a simple model for such a change in DM, we combined suitably scaled power spectra from consecutive observations of 10 minutes each. Even in this case, we did not detect any pulsed radio emission. The upper limit on the flux density of possible pulsed radio emission, based on our search, is $\sim 0.8\ \mathrm{mJy}\ (3\sigma)$.

Recent observations suggest a possible interaction between radio emission and accreted matter. It is anticipated that the system will emerge as an MSP, though strong absorption and interaction with the stellar wind are likely. Sensitive searches for pulsations should, therefore, continue.

In summary, we presented our study of pulse-to-pulse fluctuation properties of the decametric emission of a few bright pulsars based on observations at 34.5 MHz. We have used the technique of "Cartographic Transform" to study the polar emission patterns in two specific cases, viz. pulsars B0943+10 and B0834+06. We also attempted targeted searches for pulsed radio emission from two high-energy pulsars at 34.5 MHz and 327 MHz. Our observations, analysis procedures, and results were presented.

7.1 Future work

Further studies of the pulsar B0834+06 using higher frequency polarimetric data would be highly rewarding. Since our study at 34.5 MHz has allowed us to estimate of the circulation time and drift direction in the case of this pulsar reliably, studies of polar emission patterns at meter wavelengths are possible and are being attempted. Further studies of single-pulse fluctuations of the pulsars studied in the course of this thesis are possible using the GEETEE in the immediate future. Simultaneous single-pulse observations of bright pulsars using GEETEE and other telescopes, such as the ORT or GMRT, are attractive. Such observations will help to study the correspondence between polar emission regions responsible for the decametric and higher-frequency radiation.

Bibliography

[1] Alpar, A., Anderson, P., Pines, D. & Shaham J. 1984, Astrophysical Jl., 282, 791

[2] Anantharamaiah, K. R. 1984 A study of Radio Recombination Lines *From* the Galactic Plane, Ph. D. thesis, Bangalore University, India.

[3] Arendt, A. N., Eilek, J. A. 2000, preprint

[4] Arons, J., & Scharlmann, E. T. 1979, Astrophysical *Jl.*, 231, 854

[5] Asgekar A., Deshpande A. A., 2000, ASP Conference Series, Vol. 202; Proc. of IAU Colloquium # 177, (San Francisco: ASP), Ed. M. Kramer, N. Wex, and R. Wielebinski, pp. 149

[6] Asgekar, A. & Deshpande, A. A. 2001, MNRAS, 326, 1249

[7] Ashworth, M. 1982, Ph. D. thesis, University of Manchester

[8] Backer, D. C. 1973, Astrophysical *Jl.*, 182, 245

[9] Bartel, N., Sieber, W., & Wolszczan, A. 1980, Astronomy *&* Astrophysics, 90 58

[10] Beskin, V. S., Gurevich, A. V., & Istomin, Y. N. 1988, Astrophysics *&* Space Science, 146, 205

[11] Bhattacharya, D. 1997, in The Many Faces of Neutron Stars, Proc NATO-AS1 C-515, eds. Buccheri, R., Alper, A., & van Paradjis, J., pp. 103

[12] Bhattacharya, D., & van den Heuvel, E. P. J. 1991, Phys. Rep., 203, 1

[13] Burderi, L., Fauci, F., & Boriakoff, V. 1999, Astrophysical *Jl.* Letters, 512, 59

[14] Campana, S., Colpi, M., Mereghetti, S., Stella, L., & Tavani, M. 1998a, Astron. Astrophys. Rev., 8, 279

[15] Campana, S., Stella, L., Mereghetti, S., Colpi, M., Tavani, M., Ricci, D., Fiume, D. D., & Belloni, T. 1998b, Astrophysical *Jl. Letters*, 499, L65

[16] Caraveo, P. A., Bignami, G.F., Mignani, R., & Taff, L.G. 1996, Astrophysical *Jl.*, 461, L91

[17] Caraveo, P. A., Bignami, G. F., & Trümper, J. E. 1996, Astron. Astrophys. Rev., 7, 209

[18] Caraveo, P. A., Lattanzi, M. G., Massone, G., Mignani, R. P., Makarov, V. V., Perryman, M. A. C., & Bignami, G. F. 1998, Astronomy & Astrophysics, 329, L1

[19] Chakrabarty, D., & Morgan, E. H. 1998, Nature, 394, 346

[20] Chen, H.-H., Ruderman M. A., & Sutherland, P. G. 1974, Astrophysical Jl., 191, 473

[21] Cole, T. W. 1970, Nature, 227, 788

[22] Cordes, J. M. 1978, Astrophysical Jl., 222, 1006

[23] Deshpande, A. A. 1989, Technical Report on Pulsar Receiver for the GMRT, Raman Research Institute

[24] Deshpande, A. A. 2000, in Pulsar Astronomy- *2000* and beyond, IAU Colloquium 177, Ed: Kramer, M., Wex, N., & Wielebinski, R., pp. 149

[25] Deshpande, A. A., Ramachandran, R., & Radhakrishnan, V. 1999, private communication

[26] Deshpande, A. A., & Radhakrishnan, V. 1992, *Jl* Astrophys. Astr., 13, 151 (**DR92**)

[27] Deshpande, A. A., & Radhakrishnan, V. 1994, *Jl* Astrophys. Astr., 15, 329 (**DR94**)

[28] Deshpande, A. A., & Ramkumar, P. S. 1999, *Jl* Astrophys. Astr., 20, 37

[29] Deshpande, A. A., Ramkumar, P. S., & Chandrasekaran, S. 2001, under preparation

[30] Deshpande, A. A., & Rankin, J. M. 1999, Astrophysical Jl., 524, 1008 (DRa)

[31] Deshpande, A. A., & Rankin, J. M. 2001, MNRAS, 322, 438 **(Paper-I)**

[32] Deshpande, A. **A.,** Shevgaonkar, R. K., & Shastry, Ch. V. 1989, JIETE, 35, 342

[33] Dwarakanath, K. S. 1989, A Synthesis Study of the Radio Sky at Decameter Wavelengths, Ph. D. thesis, Indian Institute of Science, Bangalore, India

[34] Dwarakanath, K. S., & Udaya Shankar, N. 1990, *Jl* Astrophys. Astr., 11, 323

[35] Ferraro, V. C. A. & Plumpton, C. 1966, Magneto-Fluid Mechanics, Oxford Univ. Press, London, p. 23

[36] Gaensler, B. M., Stappers, B. W., & Getts, T. J. 1999, Astrophysical Jl. Letters, 522, 117

[37] Gil, J. A. 1987, Astrophysical *Jl.*, 314, 629

[38] Gil, J. A., Gronkowski, P., & Rudnicki, W. 1984, Astronomy & Astrophysics, 132, 312

[39] Goldreich, P. G., & Julian, W. H. 1970, Astrophysical Jl., 157, 869 (GJ)

[40] Gould, M., & Lyne, A. G. 1998, MNRAS, 301, 235

[41] Halpern, J.P., & Ruderman, M. 1993, Astrophysical *Jl.*, 415, 286

[42] Halpern, J.P., & Wang, F. Y.-H. 1997, Astrophysical Jl., 477,905

[43] Hankins, T. H. & Rickette, B. J. 1975, in Methods in Computational Physics, volume 14 (Radio Astronomy), Acedemic Press, 55

[44] Hewish, A., Bell, S. J., Pilkington, J. D. H., Scott, P. F., & Collins, R. A. 1968, Nature, 217, 709

[45] in't Zand, J. J. M., Heise, J., Muller, J. M., Bazzano, A., Cocchi, M., Natalucci, L., & Ubertini, P. 1998, Astronomy & Astrophysics, 331, L25

[46] Izvekova, V. A., Kuz'min, A. D., Malofeev, V. M., Shitov, Yu. P. 1979, *Sov.* Astron., 23, 179

[47] Izvekova, V. A., Kuzmin, A. D. & Shitov, Yu. P. 1982, *Sov.* Astron., 26, 324

[48] Kardashev, N. S., Nikolaev, N. Ya., Novikov, A. Yu., Popov, M. V., Soglasnov, V. A., Kuzmin, A. D., Smirnova, T. V., Sieber, W., Wielebinski, R. 1986, Astronomy & Astrophysics, 163, 114

[49] Kassim, N. E. & Lazio, T. J. W. 1999, Astrophysical Jl. Letters, 527, 101

[50] Komesaroff, M. M. 1970, Nature, 225, 612

[51] Kuz'min, A. D., & Losovskii, B. Ya. 1997, Astron. Lett., 23, 283

[52] Lyne, A. G., & Graham-Smith, F. 1998, Pulsar Astronomy, Cambridge University Press

[53] Lyne, A. G., & Ashworth, M. 1983, MNRAS, 204, 519

[54] Lyutikov, M., Blandford, R. D., Machabeli, G. Z. 1999, MNRAS, 305, 338

[55] Malofeev, V. M., Gill, J. A., Jessner, A., Malov, I. F., Seiradakis, J. H., Sieber, W., Wielebinski, R. 1994, Astronomy & Astrophysics, 285, 201

[56] Malofeev, V. M., & Malov, O. I. 1997, Nature, 389, 697

[57] Manchester, R. N. 1971, Astrophysical Jl. Supp. Series, 23, 283

[58] Manchester, R. N., & Taylor, J. H. 1977, Pulsars, W. H. Freeman & Co.

[59] Manchester, R. N., & Taylor, J. H. 1981, Astronomical *Jl.*, 86, 1953

[60] Mandolesi, N., Morigi, G., & Sironi, G. 1978, Astronomy & Astrophysics, 67, L5

[61] Mattox, J. R., Halpern, J. P., & Caraveo, P. A. 1996, *A&AS*, 120, 77

[62] Mayer-Hasselwander, et al. 1979, in Proc. 16^{th} Int. Cosmic Ray *Conf.*,1, 206

[63] Mayer-Hasselwander, H. A., Bertsch, D. L., Brazier, K. T. S., Chiang, J., Fichtel, C. E., Fierro, J. M., Hartman, R. C., Hunter, S. D., Kanbach, G., Kwok, P. W., Kniffen, D. A., Lin, Y. C., Mattox, J. R., Michelson, P. F., Nolan, P. L., Pinkau, K., Rothermel, H., Schneid, E. J., Sommer, M., Sreekumar, P., Thompson, D. J., von Montigny, C. 1994, 'Astrophysical *Jl.*, 421, 276

[64] McLaughlin, M. A., Cordes, J. M., Hankins, T. H., & Moffett, D. A. 1999, Astrophysical *Jl.*, 512, 929

[65] Melrose, D. B., 1995, Jl Astrophys. Astr., 16, 137

[66] Mitra, D, & Deshpande A. A. 1999, Astronomy & Astrophysics, 346, 906

[67] Nowakowski, L., Usowicz, J., Kepa, A., & Wolszczan, A. 1982, Astronomy & Astrophysics, 116, 158

[68] Nowakowski, L. 1996, Astrophysical *Jl.*, 457, 868

[69] Phillips, J. A., & Wolszczan, A. 1992, Astrophysical Jl., 385, 273

[70] Itadhakrishnan, V. A., & Cooke, D. J. 1969, Astrphys. Lett., 3, 225

[71] Radhakrishnan, V. A., & Srinivasan, G. 1982, Curr. Sci., 51, 1096

[72] Itamachandran, R., Deshpande, A. A., & Indrani, C. 1998, Astronomy & Astrophysics, 339, 787

[73] Ramkumar, P. S. 1998, Real-time Signal Processing Instrumentation for Search and Studies of Pulsars, Ph. D. thesis, Kakatiya University, Warangal, India.

[74] Ramkumar, P. S., Prabu, T., Girimaji, M., & Markandeyulu, G. 1994, Jl Astrophys. Astr., 15, 343

[75] Ramkumar, P. S., & Deshpande, A. A. 1999, *Jl* Astrophys. Astr., 20, 37

[76] Rankin, J. M. 1983a, Astrophysical *Jl.*, 274, 333

[77] Rankin, J. M. 1983b, Astrophysical *Jl.*, 274, 359

[78] Rankin, J. M. 1986, Astrophysical *Jl.*, 301, 901

[79] Rankin, J. M. 1990, Astrophysical *Jl.*, 342, 247

[80] Rankin, J. M. 1993, Astrophysical *Jl.*, 405, 285

[81] Rickette, B. J., Coles, W. A., Bourgois, G. 1984, Astronomy & Astrophysics, 134, 390

[82] Ritchings, R. T. 1976, MNRAS, 176, 249

[83] Ruderman, M. A., & Sutherland, P. G. 1975, Astrophysical Jl., 196, 51 (R&S)

[84] Ruderman, M. A. 1974, in The Physics of Dense Matter, IAU Symposium 35, Ed. Hansen, C., Reidel, pp. 117

[85] Scheure, P. A. G. 1968, Nature, 218, 920

[86] Seiradakis, J. H. 1981, Astronomy & Astrophysics, 101, 158

[87] Shitov, Yu. P. & Pugachev, V. D. 1998, New Astronomy, 3, 101

[88] Shukre, C. S., & Radhakrishnan, V. A. 1982, Astrophysical *Jl.*, 258, 121

[89] Sieber, W. 1973, Astronomy & Astrophysics, 28, 237

[90] Slee, O. B., Bobra, A. D., Alurkar, S. K. 1987, Austr. J. Phys., 40, 557

[91] Smirnova, T. V., & Boriakoff, V. 1997, Astronomy & Astrophysics, 321, 305

[92] Stairs, I. H. 1998, Observations of Binary and Millisecond Pulsars with a Baseband Recording System, Ph. D. thesis, Princeton University

[93] Stella, L., Campana, S., Mereghetti, S., Ricci, D., & Israel, G. L. 2000, Astrophysical *Jl.* Letters, 537, 115

[94] Stinebring, D. R., Cordes, J. M., Rankin, J. M., Weisberg, J. M., & Boriakoff, V. 1984, Astrophysical *Jl.* Supp. Series, 55, 247

[95] Sturrock, P. A. 1971, Astrophysical *Jl.*, 164, 529

[96] Suleymanova, S. A., Izvekova, V. A., Rankin, J. M., & Rathnasree, N. 1998, *Jl* Astrophys. Astr., 19, 1

[97] Suleymanova, S. A., Volodin, Yu. V., & Shitov, Yu. P. 1988, Sov. Astron., 32, 177

[98] Sutton, J. M. 1971, MNRAS, 155, 51

[99] Swarup, G., Kapahi, V. K., Sarma, N. V. G., Gopal-Krishna, Joshi, M. N., & Rao, A. P. 1971, Astrphys. Lett., 9, 53

[100] Taylor, J. H., & Cordes, J. M. 1993, Astrophysical *Jl.*, 411, 674

[101] Taylor, J. H., & Huguenin, G. R. 1971, Astrophysical *Jl.*, 167, 273

[102] Taylor, J. H., Manchester, R. N., & Lyne, A. G. 1993, Astrophysical *Jl.* Supp. Series, 88, 529

[103] Thompson, A. R., Moran, & J. M., Swenson Jr., G. W. 1986, Interferometry and Synthesis in Radio Astronomy, Wiley International

[104] van der Klis, M. 1997, in The Many Faces of Neutron Stars, Proc. NATO-AS1 C-515, eds. Buccheri, R., Alper, A., & van Paradjis, J., 337

[105] Vats, H. O., Singal, A. K., Deshpande, M. R., Iyer, K. N., Oza, R., Shah, C. R., & Doshi, S. 1999, MNRAS, 302, L65

[106] Vivekanand, M., Joshi, B. C. 1999, Astrophysical *Jl.*, 515, 398

[107] Vivekanand, M., Narayan, R., & Radhakrishnan, V. 1982, *Jl* Astrophys. Astr., 3, 237

[108] Walter, F. M., Wolk, S. J., & Neuhauser, R. 1996, Nature, 379, 233

[109] Wielebinski, R., Jessner, A., Kramer, M., Gil, J. A. 1993, Astronomy & Astrophysics, 272, L13

[110] Wolszczan, A. 1980, Astronomy & Astrophysics, 86, 7

[111] Weisberg, J. M., Cordes, J. M., Lundgren, S. C., Dawson, B. R., Despotes, J. T., Morgan, J. J., Weitz, K. A., Zink, E. C., Backer, D. C. 1999, Astrophysical *Jl.* Supp. Series, 121, 171

[112] Wijnands, R, & van der Klis, M. **1998, Nature, 394, 344**